

Fall 2010

Estimation of Air Flow Angles Derived from an Inertial Navigation System

Brett Douglas Mather

Embry-Riddle Aeronautical University - Daytona Beach

Follow this and additional works at: <http://commons.erau.edu/db-theses>



Part of the [Aerospace Engineering Commons](#), and the [Aviation Commons](#)

Scholarly Commons Citation

Mather, Brett Douglas, "Estimation of Air Flow Angles Derived from an Inertial Navigation System" (2010). *Theses - Daytona Beach*. Paper 134.

This thesis is brought to you for free and open access by Embry-Riddle Aeronautical University – Daytona Beach at ERAU Scholarly Commons. It has been accepted for inclusion in the Theses - Daytona Beach collection by an authorized administrator of ERAU Scholarly Commons. For more information, please contact commons@erau.edu.

ESTIMATION OF AIR FLOW ANGLES DERIVED FROM AN INERTIAL NAVIGATION SYSTEM

by

Brett Douglas Mather

A Thesis Submitted to the
Graduate Studies Office
In Partial Fulfillment of the Requirements for the
Degree of Master of Science in Aerospace Engineering

Embry-Riddle Aeronautical University
Daytona Beach, Florida
Fall 2010

UMI Number: EP31911

INFORMATION TO USERS

The quality of this reproduction is dependent upon the quality of the copy submitted. Broken or indistinct print, colored or poor quality illustrations and photographs, print bleed-through, substandard margins, and improper alignment can adversely affect reproduction.

In the unlikely event that the author did not send a complete manuscript and there are missing pages, these will be noted. Also, if unauthorized copyright material had to be removed, a note will indicate the deletion.

UMI[®]

UMI Microform EP31911
Copyright 2011 by ProQuest LLC
All rights reserved. This microform edition is protected against
unauthorized copying under Title 17, United States Code.

ProQuest LLC
789 East Eisenhower Parkway
P.O. Box 1346
Ann Arbor, MI 48106-1346

Copyright by Brett Douglas Mather 2010

All Rights Reserved

ESTIMATION OF AIR FLOW ANGLES DERIVED FROM AN INERTIAL NAVIGATION SYSTEM

by

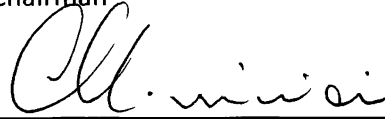
Brett Douglas Mather

This thesis was prepared under the direction of the candidate's thesis committee chairman, Dr. Richard "Pat" Anderson, Department of Aerospace Engineering, and has been approved by the members of his thesis committee. It was submitted to the Department of Aerospace Engineering and was accepted in partial fulfillment of the requirements for the degree of Master of Science in Aerospace Engineering.

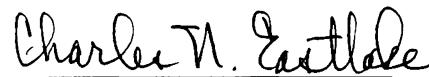
THESIS COMMITTEE:



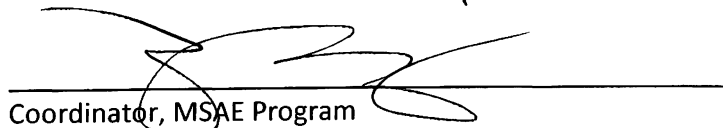
Dr. Richard "Pat" Anderson
Chairman



Dr. Maj Mirmirani
Member



Professor Charles Eastlake
Member

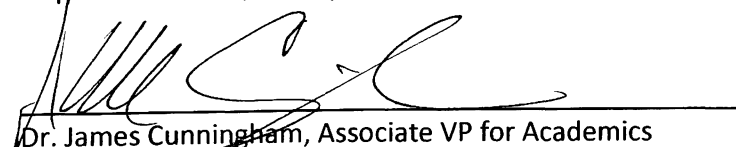


Coordinator, MSAE Program



Department Chair, Aerospace Engineering

12/3/2010
Date



Dr. James Cunningham, Associate VP for Academics

12/3/10
Date

ACKNOWLEDGMENTS

I believe that life's greatest achievements are those that at first seem impossible. This thesis would not have been possible without the many people who have helped me along the way.

I would like to thank Dr. Richard "Pat" Anderson, who took a chance in hiring me as a research assistant, but only because I was a glider pilot. Dr. Anderson gave me the opportunity to learn and experience hands-on, the dirty details of flight test engineering. My experience working with him and the talented team at Eagle Works, is the single most important take-away from my education at Embry-Riddle. As my thesis advisor, Dr. Anderson taught me things that are often neglected in the classroom, which has enabled me to become the flight test engineer I am today. He was also kind enough to endure my drawn out thesis process, and guided me to its completion by phone, email and web conferences.

I am honored to have known and to have worked with my coworkers and my classmates and Eagle Works and Embry-Riddle. I claim with great pride, that I had the opportunity to work with some of the most talented pilots, mechanics, and engineers on this planet; your futures are bright and they are yours to create.

Monica, thank you for helping me, inspiring me, and pushing me when necessary to complete this endeavor. There is no doubt, without your encouragement, this thesis would not have been finished. Our work together at Embry-Riddle solidified my knowledge, which was crucial to success at Eagle Works and on my thesis. Our aircraft discussions will forever be etched in my mind to remind me of important moments like my first flight test and earning my glider license.

To my Dad, Mom and Sister, thank you for believing in me through tough times when I didn't. Your guidance and work ethic has set me up for success no matter how difficult a challenge I may face. Your love will always empower me to do my best in all that I do.

Thanks to everyone who has been a part of my thesis, I am forever indebted to those who granted their time and knowledge to this cause.

ABSTRACT

Author: Brett Douglas Mather
Title: Estimation of Air Flow Angles Derived from an Inertial Navigation System
Institution: Embry-Riddle Aeronautical University
Degree: Master of Science in Aerospace Engineering
Year: 2007-2010

The purpose of this study is to explore the use of an Inertial Navigation System as a primary method for measuring aircraft air flow angles in flight testing. The traditional methods used to measure air flow angles consist of sensors external to the aircraft, such as an air data boom or an angle of attack probe. The advantage of using INS to measure air flow angles would be in the simplicity of the instrumentation. All components could be fixed internally, leaving minimal external modifications to the aircraft necessary for instrumentation. This would reduce costs and instrumentation time and enable air flow angle data collection in the many aircraft already fitted with an INS. Other downfalls to external sensors are the complicated calibrations and error corrections that must be used to compensate for upwash and position error of the instruments. This study will use flight test data from the Diamond DA42 Twinstar flight test program, conducted by Embry Riddle Aeronautical University. A method was developed to estimate the air flow angles using INS and other standard flight test parameters that exclude an external air data boom. This method involves determining wind velocity in order to compute an estimate for the air flow angles. Multiple Kalman Filters use air flow angle estimates to determine essential aircraft stability derivatives. Initial values for these stability derivatives are inaccurate but, over a short period of time, the Kalman Filters are able to converge to an accurate solution, provided the necessary parameters are made observable by aircraft dynamics. The converged stability derivatives are combined with aircraft accelerations to produce accurate air flow angle measurements. These air flow angles are validated against the traditionally measured air flow angles. This enables derivation of an error prediction method for INS air flow angle measurements. The predicted error is initially high, but converges along with the estimate of the stability derivatives. The methods developed in this study are implemented in a way such that real-time estimation of the air flow angles would be possible. This method is unique by focusing on instantaneous acceleration measurements while simultaneously estimating stability derivatives.

TABLE OF CONTENTS

ACKNOWLEDGMENTS	iv
ABSTRACT	v
LIST OF FIGURES	vii
LIST OF ACRONYMS	viii
NOMENCLATURE	ix
1. INTRODUCTION	1
1.1 Problem Statement	- 1
1.2 Literature Review	- 2
1.2.1 Traditional Methods.....	2
1.2.2 INS Based Modern Methods	2
1.2.3 Kalman Filtering.....	- 3 -
1.3 Hypothesis.....	- 3 -
2. METHODS	- 4 -
2.1 DA-42 Flight Test ⁹	- 4 -
2.2 AGARD ¹	- 9 -
2.3 Morelli Smoothing ⁵	- 10 -
2.4 Morelli Reconstruction ⁵	10 -
2.5 Kalman Filter to estimate bias on Angle of Sideslip	12 -
2.6 Estimating $Cy\beta$	- 13 -
2.7 Using flight path angle to estimate Angle of Attack ¹	- 16 -
2.8 Estimating $Cz\alpha$	- 17
2.9 Error prediction	19 -
3. RESULTS AND ANALYSIS	20 -
4. CONCLUSIONS	- 48 -
4.1 Parameter Identification	- 49 -
4.2 Air Flow Angle Accuracy	- 50 -
4.3 Correlation.....	- 51
4.4 Wind Estimation	- 51
4.5 Future research	- 51
5. REFERENCES	- 53 -
APPENDIX A: TEST NAMING SCHEME.....	55 -

LIST OF FIGURES

Figure 1: DA-42 Air Data Boom	- 4 -
Figure 2: AOA vane mounted to the left side of the air data boom.....	- 5 -
Figure 3: Protractor mounted behind alpha vane, calibrated in degrees up and down of the datum....	- 5 -
Figure 4: AOA Deflection vs. Voltage Ratio	- 6 -
Figure 5: AOA Upwash Calibration	7
Figure 6: Airplane Notation and Sign Convention.....	- 8 -
Figure 7: Kalman Filter to estimate bias on Angle of Sideslip	- 13 -
Figure 8: Kalman Filter to estimate $C_{y\beta}$	14 -
Figure 9: Kalman Filter to estimate $C_{z\alpha}$	18 -
Figure 10: AOS Long Duration PID Test 100 kts (2c6a1100all.csv).....	- 22
Figure 11: AOA Long Duration PID Test 100 kts (2c6a1100all.csv)	- 23 -
Figure 12: AOS Pseudo Long Duration PID Test 100 kts (2c6a1100all2.csv).....	- 24 -
Figure 13: AOA Pseudo Long Duration PID Test 100 kts (2c6a1100all2.csv)	- 25 -
Figure 14: AOS PID Test 100 kts (2c6a1100pid.csv)	- 26 -
Figure 15: AOA PID Test 100 kts (2c6a1100pid.csv).....	- 27 -
Figure 16: AOS PID Test 120 kts (2c6a1120pid.csv)	- 28 -
Figure 17: AOA PID Test 120 kts (2c6a1120pid.csv).....	- 29 -
Figure 18: AOS PID Test 75 kts (2c6a175pid.csv)	- 30 -
Figure 19: AOA PID Test 75 kts (2c6a175pid.csv).....	31
Figure 20: AOS PID Test 145 kts (2c6a1maxpid.csv)	32 -
Figure 21: AOA PID Test 145 kts (2c6a1maxpid.csv)	- 33 -
Figure 22: AOS Longitudinal Maneuvering 130 kts (2c7a1.csv)	- 34 -
Figure 23: AOA Longitudinal Maneuvering 130 kts (2c7a1.csv).....	35 -
Figure 24: AOS Dutch Roll Test 130 kts (2d7a1.csv).....	36 -
Figure 25: AOA Dutch Roll Test 130 kts (2d7a1.csv)	- 37 -
Figure 26: AOS Steady State Left Sideslip 130 kts (2d8al-correct-weight.csv).....	- 38 -
Figure 27: AOA Steady State Left Sideslip 130 kts (2d8al-correct-weight.csv)	- 39 -
Figure 28: AOS Steady State Right Sideslip 100 kts, Gear Down (2d8br.csv).....	- 40 -
Figure 29: AOA Steady State Right Sideslip 100 kts, Gear Down (2d8br.csv)	- 41
Figure 30: AOS Steady State Left Sideslip 100 kts, Gear Down (2d8bl.csv)	- 42 -
Figure 31: AOA Steady State Left Sideslip 100 kts, Gear Down (2d8bl.csv).....	- 43 -
Figure 32: AOS Steady State Left Sideslip 100 kts, Gear Down, 50% flaps (2d8cl.csv)	- 44 -
Figure 33: AOA Steady State Left Sideslip 100 kts, Gear Down, 50% flaps (2d8cl.csv).....	- 45 -
Figure 34: AOS Steady State Right Sideslip 100 kts, Gear Down, 50% flaps (2d8cr.csv).....	- 46 -
Figure 35: AOA Steady State Right Sideslip 100 kts, Gear Down, 50% flaps (2d8cr.csv)	- 47 -

LIST OF ACRONYMS

AGARD	Advisory Group for Aerospace Research and Development
ALT	Altitude
AOA	Angle of Attack
AOS	Angle of Sideslip
DATCOM	Data Compendium
ERAU	Embry-Riddle Aeronautical University
FAA	Federal Aviation Administration
FAR	Federal Aviation Regulation
GPS	Global Positioning System
IAS	Indicated Airspeed
INS	Inertial Navigation System
IMU	Inertial Measurement Unit
MATLAB	Matrix Laboratory
NASA	National Aeronautics and Space Administration
OAT	Outside Air Temperature
PC	Personal Computer
PID	Parameter Identification
PPT	Precision Pressure Transducer
SIDPAC	System Identification Programs for AirCraft

NOMENCLATURE

α	Angle of Attack
β	Angle of Sideslip
V	True Airspeed
γ	Flight Path Angle
V_N, V_E, V_D	Inertial aircraft velocities in reference to Earth (North, East, Down)
V_{W_N}, V_{W_E}	Horizontal wind velocities in reference to Earth (North and East)
V_f, V_l, V_d	Inertial aircraft velocities in reference to the air mass (Forward, Lateral, Down)
ϕ, θ, ψ	Euler Angles (Roll, Pitch, Yaw)
u, v, w	Components of velocity in the aircraft body axis in reference to the air mass
p, q, r	Components of angular velocity in the aircraft body axis
a_x, a_y, a_z	Components of acceleration in the aircraft body axis
g	Acceleration due to gravity
m	Mass of the Aircraft
ρ	Density of air mass
S	Reference wing area
X, Y, Z	Aerodynamic forces in aircraft body axis
L, M, N	Moments in the aircraft body axis
C_{z_α}	Aircraft stability derivative relating upward-force and angle of attack
C_{y_β}	Aircraft stability derivative relating side-force and angle of sideslip
C_{l_α}	Aircraft stability derivative relating lift-force and angle of attack
α_u	Un-scaled angle of attack computed from inertial measurements missing C_{z_α} factor
β_u	Un-scaled angle of sideslip computed from inertial measurements missing C_{y_β} factor
R_k	Signal Variance
Q_k	Estimated Process Noise

1. INTRODUCTION

1.1 Problem Statement

Measurements of Angle of Sideslip and Angle of Attack are some of the most important data in determining aircraft flight characteristics. These parameters, known as air flow angles, are difficult to measure because of airflow disturbance caused by the aircraft or the sensor itself. Traditionally, methods used to measure air flow angles consist of external sensors, which are moved away from the aircraft, either on a wingtip or nose boom, to minimize the airflow disturbance. Downfalls to these external sensors are the calibrations and error corrections that must be used. Upwash and sensor position error must be calibrated and corrected for in steady state tests. In dynamic maneuvers, since the air flow angles are not measured at the center of gravity of the aircraft, a correction is required for aircraft rotational motion.

Instrumentation of an aircraft to measure air flow angles is commonly expensive and time consuming. This is due to the need for aircraft modifications to install the sensors, and extensive calibration procedures for accuracy. In some cases it is impractical or impossible to traditionally instrument an aircraft to measure air flow angles. For example, hypersonic aircraft cannot make use of a traditional air data boom because it is likely that the sensors could not survive the conditions of hypersonic flight.

The research of this thesis develops a methodology for determining air flow angles without the use of traditional external sensors. The measurement of air flow angles using an Inertial Navigation System (INS) is examined as an alternative. The primary goal for this research is to derive a method to use INS data in post processing to compute air flow angles and validate them with the traditional methods. Secondly, it will be shown that this method could be used in real-time and that the associated error can be predicted to a desired confidence level.

This method would provide advantages in time and cost savings for the instrumentation of aircraft for flight test. Data measured with this method could be used to build math models of aircraft for high fidelity simulators. Additionally, many aircraft already have an INS installed or could have one added for a relatively low expense. This would make possible a wide variety of self-monitoring methods that could provide real-time air flow angle information to the control system of fly-by-wire aircraft, unmanned aircraft, or to a pilot display.

1.2 Literature Review

1.2.1 Traditional Methods

The three primary traditional methods of measuring air flow angles are vanes, null-seeking servoed differential pressure sensors, and differential pressure probes. All the traditional methods measure flow direction at their mounting location, typically on the nose of the aircraft or on an air data boom. Since these sensors are external to the aircraft, upwash and sidewash induced by the airframe require calibration between sensed flow direction and free-stream flow direction. Because the sensor is not located at the center of gravity, further calibration is required to account for aircraft dynamics. Even considering the difficulties of these traditional methods, they have been used in many flight tests and have been widely accepted as accurate when the proper instrumentation and procedures are used.¹

1.2.2 INS Based Modern Methods

Flight path reconstruction methods can use the INS measurements to estimate the air flow angles. The major downfall to flight path reconstruction for use in this particular case, is that this method relies on an initial value of the air flow angles, generally taken from an air data boom, to perform the reconstruction using INS measurements. This basic method typically suffers from random walk, due to a very small bias present in all accelerometers being integrated over time, thus introducing a growing error in the solution over time.⁵

Work has been done attempting to use inertial accelerations to estimate air flow angles. This type of research is enabled by the increased affordability of high accuracy INS units. Dr. Colgren performed a study to research the potential of using INS to replace air data probes on high performance aircraft for control system feedback. The study used flight test data and simulators in an attempt to show the feasibility of replacing air data probes with INS measurements. This was a daunting task, due to the high accuracy of air flow angles required for proper control system feedback. The conclusion was that the INS measurements were not sufficient to replace the air data system due to difficulty in gust estimation.²

In a study of the U2S aircraft, the concept was employed and shown to be feasible for estimating sideslip angle for flight test measurements rather than control system feedback. This case concludes that the method works well, but is likely due to the large lateral surface area of the U2S making lateral

accelerations more prominent and easier to measure.^{3, 4} Studies of this nature have shown promising results, but none have done extensive testing with publicly available data on the overall accuracy.

1.2.3 Kalman Filtering

A Kalman Filter is a recursive method that estimates the state of a system from noisy measurements. The Kalman Filter essentially predicts the state at the next time step, and then corrects its estimate based on that prediction. The filter then converges to an optimal solution by minimizing the error covariance. The Kalman filter has been widely used since R. E. Kalman published his filter derivation in 1960. It was during Kalman's visit to the NASA Ames Research Center that he saw the usefulness of his ideas to the trajectory estimation for the Apollo program, leading to its incorporation in the Apollo navigation computer. Kalman filtering applies to a broad range of subjects, including engineering control systems, radar, and economics.^{6, 7, 8}

Kalman filter gain logic is the key to a basic understanding of how the filter works. The input of process noise to the filter is essentially a measure of confidence in the measurement being input at the same time. Therefore, if a high process noise is input, it would represent a high confidence in the measurements over the filter's current model it is using to estimate the solution. Conversely, low process noise would correspond to low confidence in the measurement and the filter's model would be trusted more. With this information being given to the filter, it operates recursively, updating its model with each iteration based on the confidence input of the measurement at a given time.⁶

With this understanding of the Kalman filter, it can be tuned by altering the inputs given for the process noise. A higher process noise, essentially higher confidence in the current measurement, will result in quicker convergence of the filter, while the opposite, lower process noise, would cause the filter to converge slowly, or possibly to diverge. Choosing proper values for the input of process noise for a basic user is easily done with a process of tuning via trial and error.⁶

1.3 Hypothesis

Using flight test data, a method can be devised to compute air flow angles to replace traditional methods of measuring air flow angles. This method will be expressed in the form of a computer algorithm to compute the air flow angles, and their associated error. This software could be used in flight testing scenarios when an engineer must see the air flow angles in flight. In static cases, it is likely that the error will increase with time; maneuvers to make these parameters observable may be

necessary to continually calibrate the air flow angles on the fly. Additionally, the unknown atmospheric turbulence is the most crucial uncertainty, but by estimating the stability derivatives and using them to estimate the air flow angles, the effects of this uncertainty are minimized.

This method will be validated using flight test data that includes air flow angles from an air data boom. Pseudo-real-time calculations of the air flow angles will be compared to direct measurements of the air flow angles with the air data boom to quantify error, and to show that this method could be used to replace traditional methods of measuring air flow angles.

2. METHODS

The method designed to test this hypothesis makes use of flight test data obtained from Embry-Riddle Aeronautical University on the Diamond DA42 Twinstar aircraft. This data contains traditional measurement of air flow angles, and all necessary data to compute another version of these air flow angles using primarily INS measurements. The algorithms and methods included were all developed in Mathworks MATLAB and Simulink computing environments.

2.1 DA-42 Flight Test⁹

The flight test data used to create and test this method are from the Diamond Twinstar DA-42 flight test performed by Embry-Riddle Aeronautical University. This data was collected using a typical air data boom with potentiometer vanes for angle of attack and angle of sideslip. In addition, a Novatel ring laser gyro based IMU and differential GPS are coupled with a Kalman filter to provide INS data. Honeywell precision pressure transducers measure airspeed and altitude. All the data were collected on a PC running National Instruments Labview software at a rate of 20Hz.



Figure 1: DA-42 Air Data Boom



Figure 2: AOA vane mounted to the left side of the air data boom

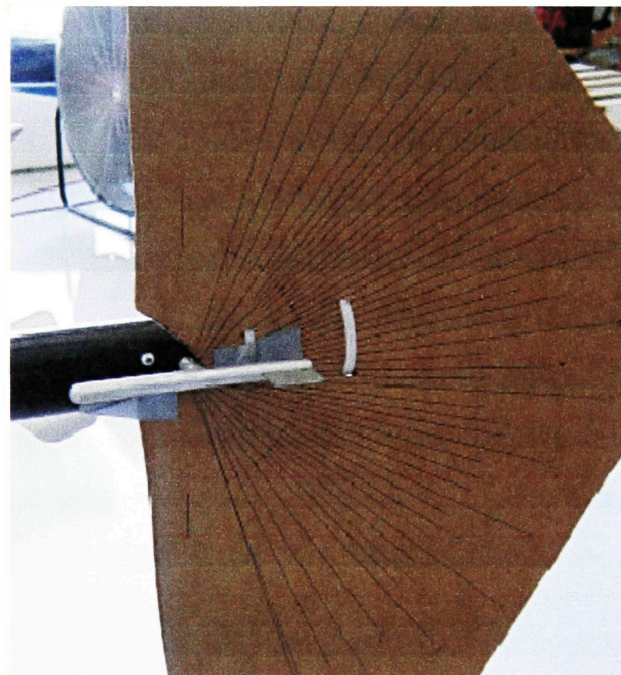


Figure 3: Protractor mounted behind alpha vane, calibrated in degrees up and down of the datum

An example of calibration for AOA is included from the DA-42 Flight Test Report. The following graph shows the relationship between the deflection angle of the angle of attack vane and the ratio of the voltage at the potentiometer to the excitation voltage.

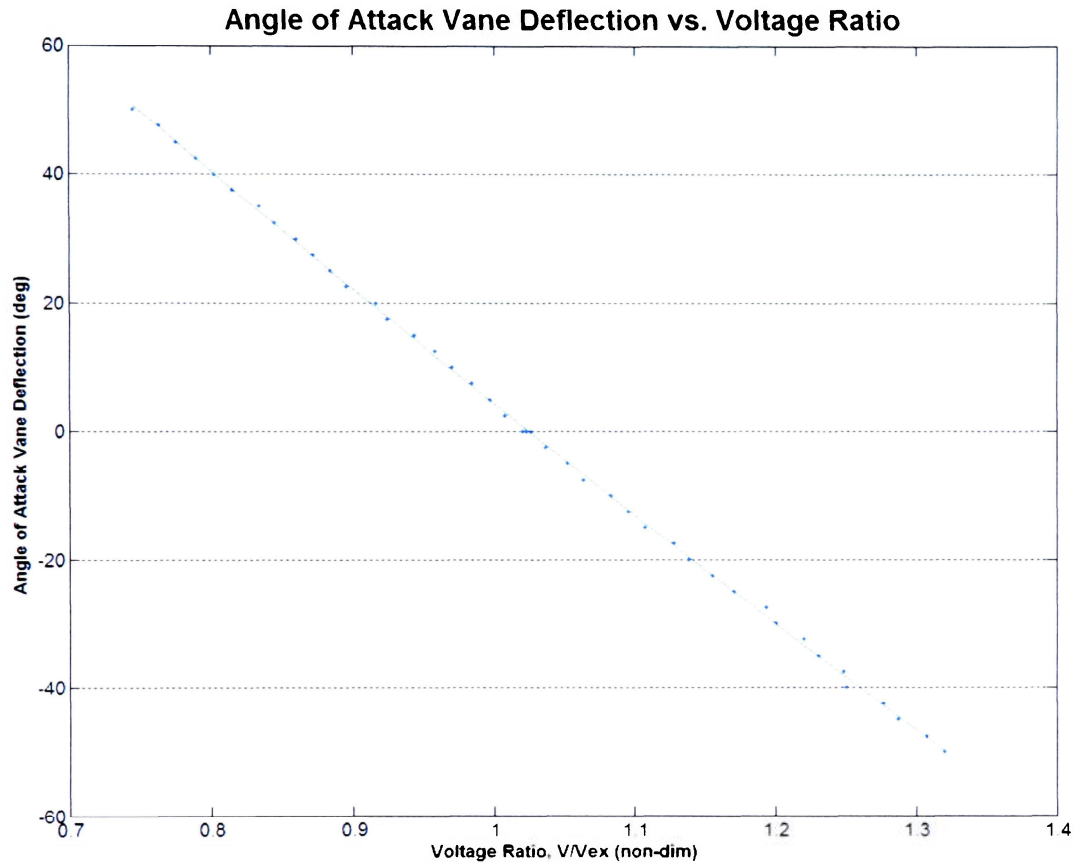


Figure 4: AOA Deflection vs. Voltage Ratio

After relating degrees of deflection for the transducer to a voltage ratio, the second calibration is needed. This is the calibration that takes into account upwash effect on the sensor in flight.

Calibration was done in level flight at different airspeeds with no flaps and gear up. In level flight, the change in pitch should be the same as the change in the angle of attack. If there are any discrepancies, it indicates that an upwash effect exists at the angle of attack vane. Therefore,

$$\alpha_{boom} = \theta \left(1 + \frac{\partial \epsilon}{\partial \alpha} \right),$$

where pitch is equal to theta or angle of attack true.

Rearranging the previous equation:

$$\frac{\partial \varepsilon}{\partial \alpha} = 1 - \frac{\alpha_{boom}}{\theta}$$

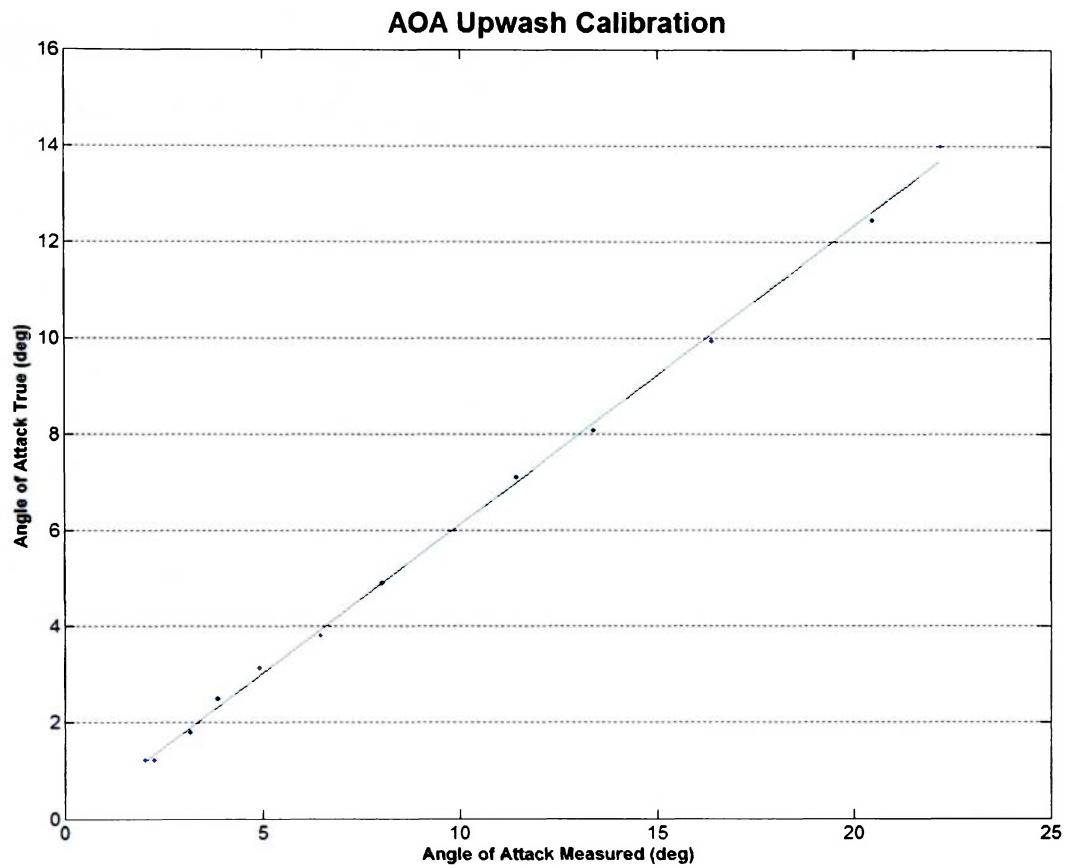


Figure 5: AOA Upwash Calibration

The measured AOA can only be related to the true AOA after significant flight testing. This method of calibration was performed additionally for AOA and AOS for each combination of flap and gear configurations with a total of 12 calibrations. The meticulous and lengthy process required for these calibrations is one of the most obvious reasons for attempting to find a better way to measure air flow angles.

Variable	Instrument	Accuracy
Time	SPAN GPS/IMU INS	20 ns
IAS	Honeywell Precision Pressure Transducer (PPT)	0.01 psi
True airspeed (V)	Computed from: IAS, OAT, alt	Corrected for position error and density altitude
Altitude (h)	Honeywell Precision Pressure Transducer (PPT)	0.01 psi
Alpha (α)	Vane/Potentiometer 6538S-1-103 LIN	+/-10% resistance +/-1% independent linearity
Beta (β)	Vane/Potentiometer 6538S-1-103 LIN	+/-10% resistance +/-1% independent linearity
Roll rate (p)	SPAN GPS/IMU INS	--
Pitch rate (q)	SPAN GPS/IMU INS	--
Yaw rate (r)	SPAN GPS/IMU INS	--
Roll angle (ϕ)	SPAN GPS/IMU INS	0.015 deg
Pitch angle (θ)	SPAN GPS/IMU INS	0.015 deg
Yaw angle (ψ)	SPAN GPS/IMU INS	0.05 deg
Longitudinal acceleration (a_x)	SPAN GPS/IMU INS	0.003g
Lateral acceleration (a_y)	SPAN GPS/IMU INS	0.003g
Normal acceleration (a_z)	SPAN GPS/IMU INS	0.003g

Pertinent DA42 Data Parameters

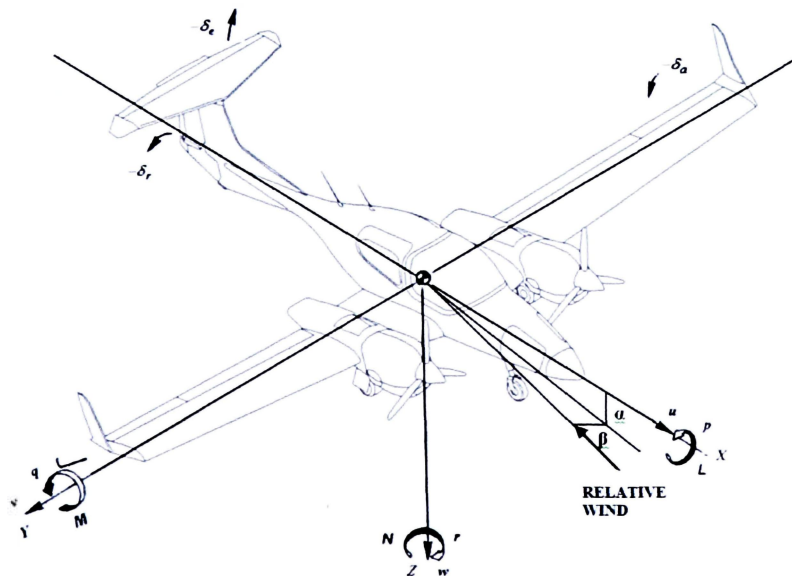


Figure 6: Airplane Notation and Sign Convention

2.2 AGARD¹

The AGARD (Advisory Group for Aerospace Research and Development) method for computing wind speed and direction uses error minimization between true airspeed and the INS-measured groundspeed. Newton-Raphson iterations are necessary to converge to a solution for the wind. This method was extended to work in pseudo-real-time as a window of data to compute wind speed and direction, but was shown to yield better results if the wind was estimated as a constant throughout the maneuver. It should be possible to use a real-time estimation of wind velocity to improve the overall estimate of the air flow angles. The results of the wind calculation were compared to manually calculated wind velocities for certain tests in order to validate the method. The AGARD method is described in the following:

$$V_f = V_N - V_{WN}$$

$$V_l = V_E - V_{WE}$$

$$V_d = V_D$$

V_N , V_E , and V_D are ground speeds measured with an INS; V_{WN} and V_{WE} are the components of the wind; V_f , V_l , and V_d are forward, lateral, and down components of velocity. It should be noted that this method of wind estimation assumes there is no vertical wind present. This is generally considered a good assumption, since vertical winds are short-lived and inconsistent. Flight tests of this nature must be performed in calm conditions, near zero vertical wind, to obtain worthy results. The following equation relates the true airspeed, V , to the INS velocities:

$$V^2 = (V_N - V_{WN})^2 + (V_E - V_{WE})^2 + V_D^2$$

The sum of the squares of the residual errors in true airspeed over the entire maneuver is below:

$$ERRSUM = \sum_{j=1}^N \left[V_j^2 - (V_{Nj} - V_{WN})^2 - (V_{Ej} - V_{WE})^2 - V_{Dj}^2 \right]^2$$

Values for V_{W_N} and V_{W_E} are chosen to minimize this error, which will occur when the following partial derivative equations are equal to zero. These equations can be solved simultaneously using a 2D Newton-Raphson iteration.

$$\frac{\partial ERRSUM}{\partial V_{W_N}} = \sum_{j=1}^N \left[V_j^2 - (V_{N_j} - V_{W_N})^2 - (V_{E_j} - V_{W_E})^2 - V_{D_j} \right] (V_{N_j} - V_{W_N}) = 0$$

$$\frac{\partial ERRSUM}{\partial V_{W_E}} = \sum_{j=1}^N \left[V_j^2 - (V_{N_j} - V_{W_N})^2 - (V_{E_j} - V_{W_E})^2 - V_{D_j} \right] (V_{E_j} - V_{W_E}) = 0$$

Now with the wind estimated, the air mass velocities must be transformed in the body axis via the following rotation matrix:

$$\begin{bmatrix} u \\ v \\ w \end{bmatrix} = \begin{bmatrix} \cos\theta\cos\psi & \cos\theta\sin\psi & -\sin\theta \\ \cos\phi\sin\psi + \sin\theta\sin\phi\cos\psi & \sin\theta\sin\phi\sin\psi + \cos\phi\cos\psi & \cos\theta\sin\phi \\ \sin\theta\cos\phi\cos\psi + \sin\phi\sin\psi & \sin\theta\cos\phi\sin\psi - \sin\phi\cos\psi & \cos\theta\cos\phi \end{bmatrix} \begin{bmatrix} V_f \\ V_l \\ V_d \end{bmatrix}$$

Finally, the solution is found with the classic angle of attack and angle of sideslip equations:

$$V = \sqrt{u^2 + v^2 + w^2}$$

$$\beta = \sin^{-1}\left(\frac{v}{V}\right)$$

$$\alpha = \tan^{-1}\left(\frac{w}{u}\right)$$

2.3 Morelli Smoothing⁵

Acceleration data acquired from the INS is inherently noisy, due to the high rate of data acquisition as compared to the dynamics of the aircraft. Data used from this flight test were recorded at 20Hz, which tended to be noisy enough to create difficulty in determining the accuracy of the method. To combat this, a low pass smoothing filter from SIDPAC was implemented. This MATLAB function was edited by graduate student Chris Brown to enable a hardcoded cut-off frequency for the filter.

2.4 Morelli Reconstruction⁵

Morelli's method for reconstructing angle of attack and angle of sideslip are fundamental to estimating these angles without an air data boom. This method currently relies on an air data boom for

its initial values, but then uses the equations of motion to discretely integrate a reconstructed solution for the air flow angles. This method does an excellent job of estimating air flow angles, but is subject to random walk, due to integration of accelerations measured from slightly biased accelerometers. This error builds over time and makes the reconstruction unusable. The method is described as follows:

$$\begin{aligned}\beta_0 &= \beta \\ \alpha_0 &= \alpha\end{aligned}$$

The initial angle of attack and angle of sideslip values are taken from the air data boom, and then used along with true airspeed to obtain initial body axis velocities.

$$x_0 = V \times \begin{bmatrix} \cos(\alpha_0) \cos(\beta_0) \\ \sin(\beta_0) \\ \sin(\alpha_0) \cos(\beta_0) \end{bmatrix}$$

$$x_0 = \begin{bmatrix} u_0 \\ v_0 \\ w_0 \end{bmatrix}$$

Next, the change in body axis velocities is computed using the equations of motion:

$$\begin{aligned}u' &= rv - qw - g \sin(\theta) + a_x \\ v' &= -ru + pw + g \cos(\theta) \sin(\phi) + a_y \\ w' &= qu - pv + g \cos(\theta) \cos(\phi) + a_z\end{aligned}$$

A 4th order Runge-Kutta integration is performed to yield the body axis velocities for the next time step.

$$x = \begin{bmatrix} u \\ v \\ w \end{bmatrix}$$

In the final step the reconstructed true airspeed, angle of sideslip, and angle of attack are computed from the reconstructed body axis velocities.

$$V = \sqrt{u^2 + v^2 + w^2}$$

$$\beta = \sin^{-1}\left(\frac{v}{V}\right)$$

$$\alpha = \tan^{-1}\left(\frac{w}{u}\right)$$

This process is repeated as an iterative method to reconstruct data for each time step throughout the maneuver.

2.5 Kalman Filter to estimate bias on Angle of Sideslip

The first step in developing a new method to estimate air flow angles began with estimating a bias on the angle of sideslip. A Kalman filter was used to estimate the bias on the angle of sideslip computed from the AGARD wind estimation method. This method exploits the notion that when a_y is zero, β is also zero. In this method, the Kalman filter is constantly fed the difference between β and a_y and designed to estimate this difference as a constant bias on β . The R_k values fed to the Kalman filter correspond to the confidence in the bias being fed to the filter. When a_y is within ± 0.0025 g's (approximately zero), the R_k value is set to $1e-15$ to give the filter extremely high confidence in the bias at that time step. Conversely, when a_y is outside the range of ± 0.0025 g's (considered to be non-zero), the R_k value is set to $9e9$ to give the filter extremely low confidence in the bias at this time step.

As the filter continually receives the bias and its confidence in that bias, it converges on a value for the bias. This bias is then removed from the β calculated by the AGARD wind estimation method to yield an accurate estimate of β . This method of using the filter is shown in the following Simulink model:

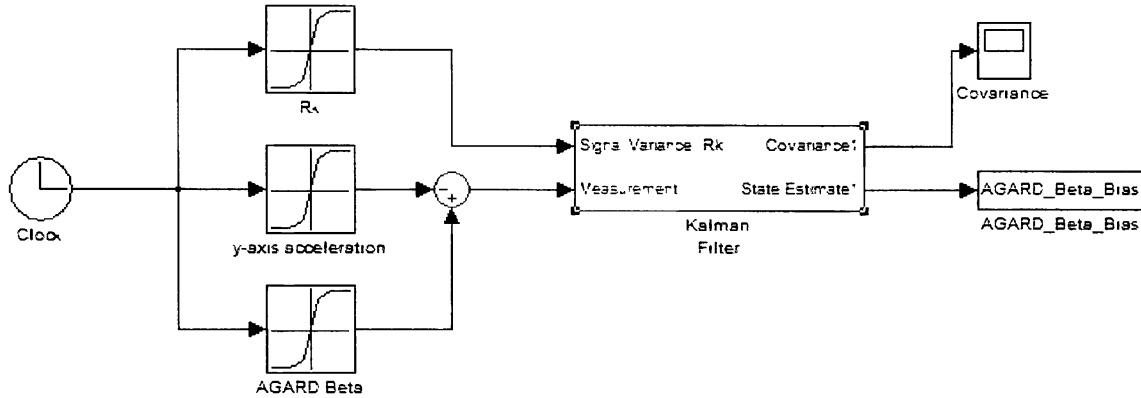


Figure 7: Kalman Filter to estimate bias on Angle of Sideslip

2.6 Estimating $C_{y\beta}$

With a method in place to estimate the bias on AOS, next a method to estimate the scale factor was necessary. This scale factor being estimate is essentially $C_{y\beta}$. Sideslip angle and side force are related by:

$$Y = \frac{1}{2} \rho V^2 S C_{y\beta} \beta$$

Estimation of sideslip angle using the INS can be achieved using the following equation:

$$\beta = \frac{a_y m}{\frac{1}{2} \rho V^2 S} \cdot \frac{1}{C_{y\beta}}$$

a_y is the lateral acceleration, m is aircraft mass, $\frac{1}{2} \rho V^2$ is dynamic pressure, and S is wing area. All of the values other than β , a_y , and $\frac{1}{2} \rho V^2$ can be considered constant for a short flight test maneuver. Dynamic pressure is easily calculated from the airspeed, altitude, and temperature measurements, normally recorded during a flight test. Wing area is a relatively well-known value on any modern aircraft and the aircraft's instantaneous mass can be calculated in a number of ways using modern flight test

procedures. Lateral acceleration, a_y , is recorded directly from the IMU to a high degree of accuracy. This leaves $C_{y\beta}$ and β as the only unknown values. A method for estimating $C_{y\beta}$ in real-time would allow β to be calculated from acceleration and dynamic pressure directly. A proposed method for estimating $C_{y\beta}$, and then β , is shown in the simulink model below:

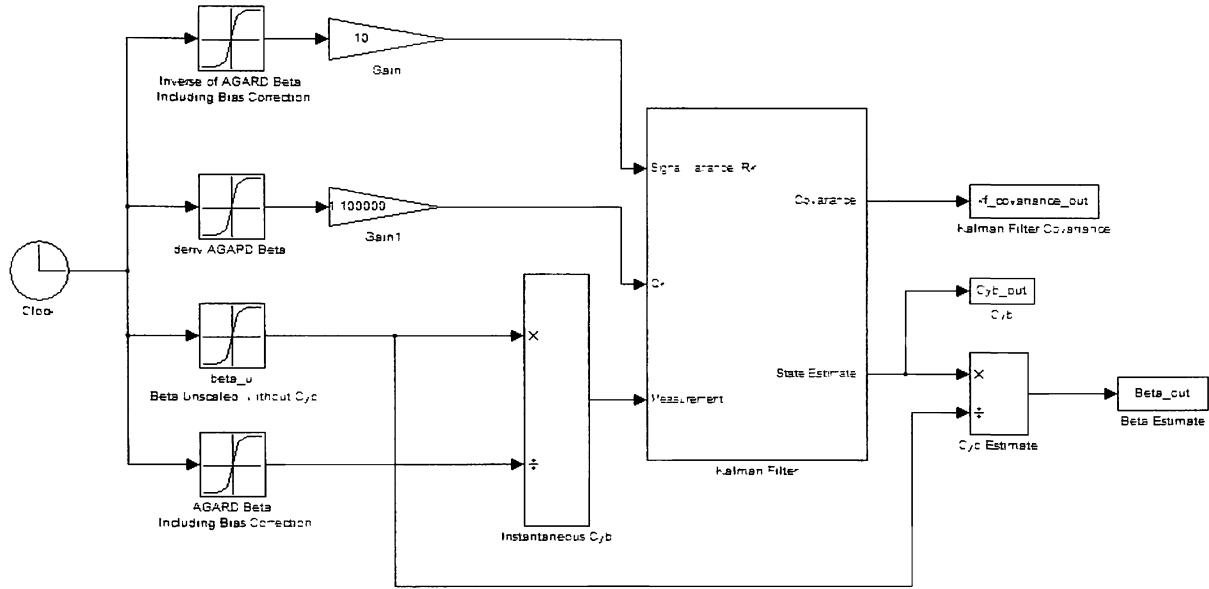


Figure 8: Kalman Filter to estimate $C_{y\beta}$

In this method, the Kalman filter has been tuned using the R_k and Q_k inputs. The inverse of sideslip angle measured from the AGARD method is input for the Signal Variance, R_k . It should be noted that this sideslip angle value is already corrected for a bias, as described previously. This means when there is a high value for β it will be inverted and go into the Kalman filter as a low value corresponding to high confidence in the measurement for that time step. The gain of ten (10) on the signal is a matter of tuning the filter. Using a higher gain causes the filter to converge more slowly, but yields a more accurate final answer. A lower gain causes the filter to converge more quickly, but sacrifices in the fact that the filter estimate will contain more noise.

The filter is fed the Q_k value of the derivative of sideslip angle from the AGARD method. A high value for Q_k implies high confidence in the measurement (the opposite of R_k). So this means that if the rate of change of β is high, then there is higher confidence in the measurement. The gain used to tune Q_k is $1/1000000$, which causes Q_k to have only a small effect on the estimate.

The third parameter input to the Kalman filter in this scenario is an instantaneous $C_{y\beta}$. In this case of the DA-42, the initial value for $C_{y\beta}$ is set to the value that was found using DATCOM analysis of the airframe.¹⁰ Using DATCOM, or a similar method, to find an initial guess for $C_{y\beta}$ is relatively simple, and allows the Kalman filter to converge much more easily; however, even with no initial guess, the filter will still converge properly, as long as the stability derivatives are made observable through maneuvers. The initial value used for $C_{y\beta}$ in the DA-42 is -0.4. This value is fed to the Kalman filter with a very high confidence--an R_k of 1000. After this initial guess of $C_{y\beta}$, the filter continues to run using actual flight test data. Instantaneous estimates for $C_{y\beta}$ are obtained using the following equations:

It has already been shown that:

$$\beta = \frac{a_y m}{\frac{1}{2} \rho V^2 S} \cdot \frac{1}{C_{y\beta}}$$

This value of β can come from the AGARD method. So if an un-scaled angle of sideslip is calculated from measured parameters, but $C_{y\beta}$ is excluded, we get:

$$\beta_u = \frac{a_y m}{\frac{1}{2} \rho V^2 S}$$

Next the un-scaled β_u is divided by the β computed from the AGARD method to yield an instantaneous value of $C_{y\beta}$:

$$C_{y\beta} = \frac{\beta_u}{\beta} = \frac{\left(\frac{a_y m}{\frac{1}{2} \rho V^2 S} \right)}{\left(\frac{a_y m}{\frac{1}{2} \rho V^2 S} \cdot \frac{1}{C_{y\beta}} \right)}$$

Now that an instantaneous value for $C_{y\beta}$ is being computed, it is fed to the Kalman filter with the previously mentioned R_k and Q_k confidence values. The Kalman filter then will estimate $C_{y\beta}$ as a constant value, based on the confidence of each measurement, and will converge to a solution. The solution for $C_{y\beta}$ will initially contain a large error. As dynamic aircraft movements occur, the higher confidence values of R_k and Q_k will be seen and the filter will obtain an optimal solution.

This estimated value for $C_{y\beta}$ is then inversed and multiplied back into the un-scaled β to obtain an actual estimate of sideslip angle.

$$\beta_u \left(\frac{1}{C_{y\beta}} \right) = \frac{a_y m}{\frac{1}{2} \rho V^2 S} \cdot \frac{1}{C_{y\beta}} = \beta$$

2.7 Using flight path angle to estimate Angle of Attack¹

In order to estimate angle of attack, a method traditionally used to calibrate angle of attack vanes is employed. This method involves computing the aircraft's flight path angle, γ , directly from INS measurements. First the horizontal speed is computed from North and East velocities:

$$V = \sqrt{V_N^2 + V_E^2}$$

Next, flight path angle can be computed using the upward velocity and the horizontal speed.

$$\gamma = \tan^{-1} \left(\frac{V_U}{V} \right)$$

Finally, an estimate for angle of attack is found from the computed flight path angle and pitch angle which is directly measured from the INS.

$$\alpha = \theta - \gamma$$

This method comes with some important assumptions, the first being zero vertical wind. This assumption is valid for most flight testing, as test programs should be performed on calm days with no turbulence. The second major assumption for this method is zero bank angle. With any significant bank angle, this method breaks down and flight path angle calculations are inaccurate. This assumption is quite limiting as to which maneuvers angle of attack can be estimated.

Although experimentation was performed using this method as an initial guess for angle of attack, it was found that using the INS measurements along with the AGARD method to estimate the wind as an initial guess for angle of attack, yielded better results.

2.8 Estimating $C_{z\alpha}$

A Kalman Filter is used in the same manner as the Kalman Filter that estimates $C_{y\beta}$ but it is now set up to estimate $C_{z\alpha}$. Since estimation of $C_{z\alpha}$ is very similar to the estimation of $C_{y\beta}$, this section will have a less rigorous explanation of the method and will be nearly identical to the section on estimating $C_{y\beta}$.

Just as in the estimation of $C_{y\beta}$, the initial guess for the air flow angle comes from the AGARD method. One significant difference for the estimation of $C_{z\alpha}$ is due to the non-zero angle of attack at the start of the test. At the beginning of each test, a few seconds of data is recorded while the aircraft is flown in a trimmed condition. Generally, this condition will have a positive value for angle of attack. For this method to work properly, this trim angle of attack is removed temporarily for use in the Kalman filter. Since the filter works based on how far the angle of attack is from zero, we must make the filter believe the trim angle of attack is zero. The initial angle of attack is found by averaging the first ten data points. Next, this initial angle of attack is subtracted from each data point throughout the file, essentially removing it as a bias, moving the trim angle of attack to zero. Then the Kalman filter is run with this new angle of attack, and generates an estimated angle of attack. The initial angle of attack averaged from the first ten data points is then added back in to the filter's estimate, since it would be improper to leave this bias out. This bias removal and replacement are not shown in the following method explanation.

Angle of attack and upward force are related by:

$$Z = \frac{1}{2} \rho V^2 S C_{z\alpha} \alpha$$

Estimation of angle of attack using the INS can be achieved using the following equation:

$$\alpha = \frac{a_z m}{\frac{1}{2} \rho V^2 S} \cdot \frac{1}{C_{z\alpha}}$$

Next, the Kalman filter is used to estimate $C_{z\alpha}$ and then α :

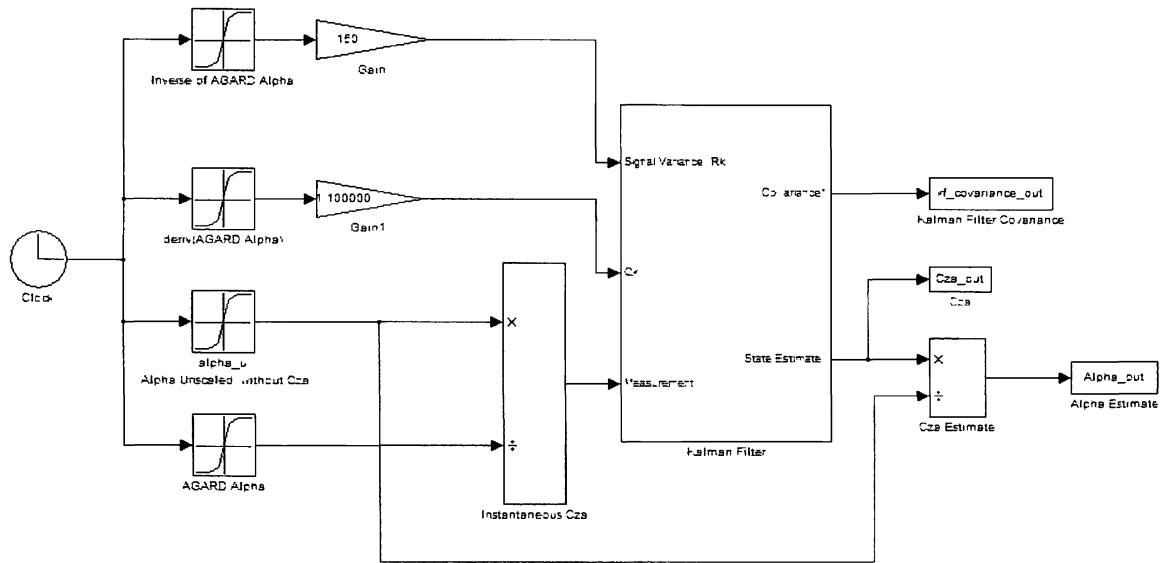


Figure 9: Kalman Filter to estimate C_{z_α}

The Kalman filter is tuned, as previously explained in the estimation of C_{y_β} section. This tuning deals with the first two input parameters, R_k and Q_k , for the filter. One difference in the tuning of this C_{z_α} filter is the gain for R_k was changed to 150. The third parameter input to the Kalman filter in this scenario is an instantaneous C_{z_α} . In the case of the DA42, the initial value for C_{z_α} is set to the value that was found using DATCOM analysis of the airframe (the value from DATCOM was for C_{l_α} , but in this case it is accurate enough to serve as an initial guess for C_{z_α}).¹⁰ Using DATCOM, or a similar method, to find an initial guess for C_{z_α} is relatively simple, and allows the Kalman filter to converge much more easily; however, even with no initial guess, the filter will still converge properly, as long as the stability derivatives are made observable through maneuvers. The initial value used for C_{z_α} in the DA-42 is -5.7. This value is fed to the Kalman filter with a very high confidence--an R_k of 1000. After this initial guess of C_{z_α} is input, the filter continues to run using actual flight test data. Instantaneous estimates for C_{z_α} are obtained using the following equations:

It has already been shown that:

$$\alpha = \frac{a_z m}{\frac{1}{2} \rho V^2 S} \cdot \frac{1}{C_{z_\alpha}}$$

This initial value of α can come from the AGARD method previously described. So if an un-scaled angle of attack is calculated from measured parameters, but $C_{z\alpha}$ is excluded, we get:

$$\alpha_u = \frac{a_z m}{\frac{1}{2} \rho V^2 S}$$

Next, the un-scaled α_u is divided by the α computed from the flight path angle method to yield an instantaneous value for $C_{z\alpha}$:

$$C_{z\alpha} = \frac{\alpha_u}{\alpha} = \frac{\left(\frac{a_z m}{\frac{1}{2} \rho V^2 S} \right)}{\left(\frac{a_z m}{\frac{1}{2} \rho V^2 S} \cdot \frac{1}{C_{z\alpha}} \right)}$$

Now that an instantaneous value for $C_{z\alpha}$ is computed, it is fed to the Kalman filter with the previously mentioned R_k and Q_k confidence values. The Kalman filter then will estimate $C_{z\alpha}$ as a constant value, based on the confidence of each measurement and converge to a solution.

This estimated value for $C_{z\alpha}$ is then inversed and multiplied back into the un-scaled α to obtain an actual estimate for angle of attack.

$$\alpha_u \left(\frac{1}{C_{z\alpha}} \right) = \frac{a_z m}{\frac{1}{2} \rho V^2 S} \cdot \frac{1}{C_{z\alpha}} = \alpha$$

2.9 Error prediction

For a method of this nature to be useful in flight testing, a confidence in the estimated value of the air flow angle must be available. From empirical evidence, the following equation was derived:

$$Error Prediction = \frac{\left| \frac{\partial C_{y\beta}}{C_{y\beta}} \right|}{Kalman Covariance}$$

The error prediction can be defined as predicted error in degrees of sideslip angle. In this error prediction, $\partial C_{y\beta}$ is the primary driving factor. The plot of $\partial C_{y\beta}$ correlates to the actual error very well. This makes sense because, if the Kalman filter is estimating $C_{y\beta}$ as changing drastically, then it is likely

that the estimation of $C_{y\beta}$ at that time is inaccurate. Large change in $C_{y\beta}$ literally means $\partial C_{y\beta}$ would be a relatively large value, thus corresponding to large error.

The Kalman covariance is output from the Kalman filter, along with the estimate of the air flow angle. This value generally converges asymptotically towards zero. It was observed that $\partial C_{y\beta}$ over-estimates the error when the Kalman covariance is greater than one. Concurrently, it was observed that $\partial C_{y\beta}$ under-estimates the error when the Kalman covariance is less than one. This observation brought about the conclusion that dividing by the Kalman covariance would increase the error measurement when $\partial C_{y\beta}$ was under-estimating, and would decrease the error measurement when $\partial C_{y\beta}$ was over-estimating.

The inclusion of $C_{y\beta}$ in the error prediction serves the purpose of driving the initial error higher. Initial estimates for $C_{y\beta}$ are inherently wrong until the Kalman filter has sufficient time to converge to an accurate value. With the initial estimate for $C_{y\beta}$ being relatively infinite, adding this parameter drives the predicted error sufficiently higher in first seconds of the filter running.

A first order regression filter was employed to smooth the error prediction, and to remove anomalies that occur in the prediction. This smoothing is necessary only to neaten the appearance of the predicted error.

The same error prediction equation is employed for $C_{z\alpha}$. Gains of 2 and 60 were added to the predicted error equations for $C_{y\beta}$ and $C_{z\alpha}$ respectively, to more closely reach a 95% confidence level.

3. RESULTS AND ANALYSIS

The results of this method are displayed in this section using output graphs from the MATLAB code. Each figure shows a graph of the air flow angle (sideslip angle or angle of attack) measured with both the air data boom and with this new estimation method. Each figure also shows a second graph of the error in degrees between the air data boom's measurement and this method's estimation. On this second graph, the predicted error from the estimation is also plotted so that the actual error and the predicted error are compared. The number in the legend corresponding to actual error is the average of the absolute error for the test in degrees; the number corresponding to predicted error is the

percentage of confidence in the error prediction for the given test. A third graph shows the Kalman Filter's estimation of the stability derivative ($C_{y\beta}$ or $C_{z\alpha}$), along with an accepted value from previous research.

Values for $C_{y\beta}$ and $C_{z\alpha}$ were obtained from research with the purpose of determining the stability and control derivatives for the DA-42 aircraft. This research was performed using the same set of DA-42 flight test data. The values were computed using parameter identification methods involving the SIDPAC data analysis tools. The value for $C_{z\alpha}$ was not calculated in the research, so $C_{l\alpha}$ was assumed to be roughly equivalent and this value was used for comparison. The value obtained for $C_{z\alpha}$ was -4.7 and the value for $C_{y\beta}$ was -0.28.¹⁰

Figure titles explain which parameter is being estimated (AOA or AOS) and the test name, speed and configuration. The figure captions are the data filenames from which the naming scheme is drawn out in detail in Appendix A. The flight test maneuvers performed in the DA-42 follow guidance from FAR Part 60. The PID maneuver consists of a 3-2-1-1 pitch maneuver, followed by a rudder doublet, followed by an aileron doublet. All tests used in this study were in flaps up and gear up, cruise configuration unless otherwise indicated. Speeds shown are indicated airspeed at the start of the test.

The first example in Figure 10 shows an AOS for a PID test maneuver with a long duration steady state prior to the maneuver. Initially, the Kalman filter is predicting large error in its estimation, due to the fact that the parameters being estimated have not been excited to the point that would make them observable. Convergence is seen during the first 25 seconds, at which point the convergence stabilizes and maintains throughout the rest of this test. The filter's estimate of $C_{y\beta}$ converges to a value of approximately -0.28, which is found in a previous DA-42 PID measurement of $C_{y\beta}$.¹⁰

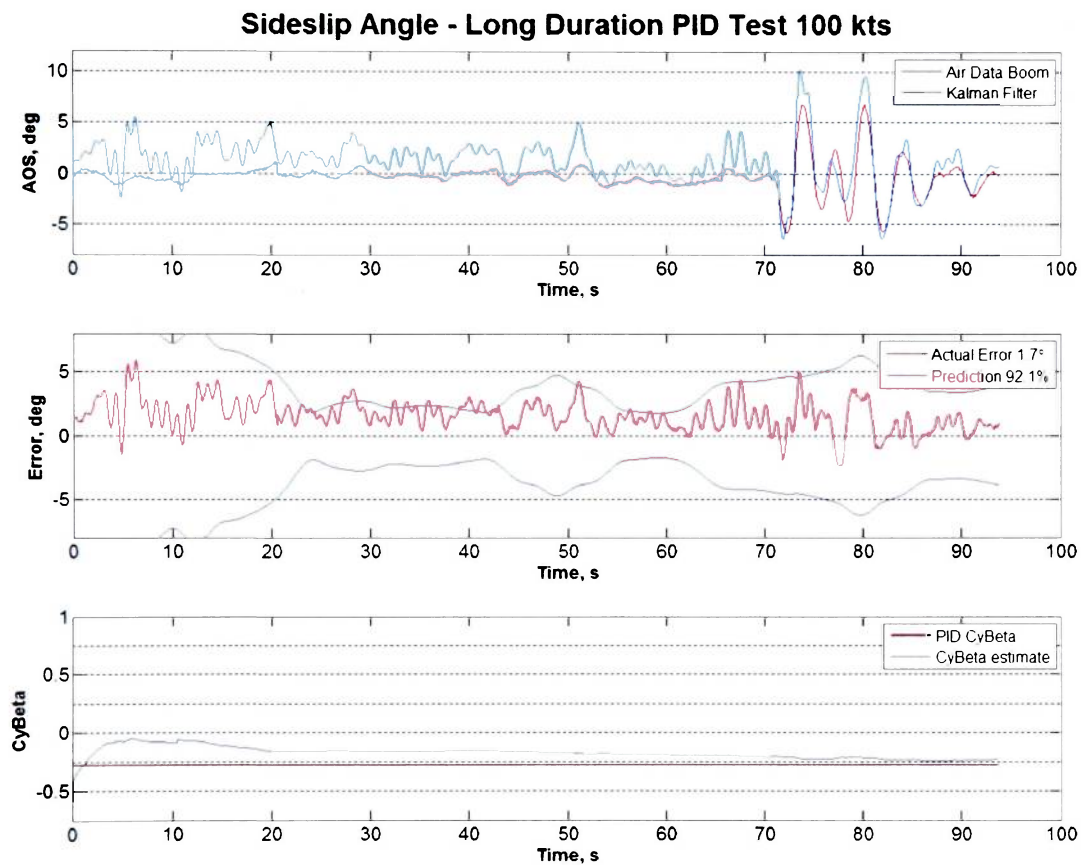


Figure 10: AOS Long Duration PID Test 100 kts (2c6a1100all.csv)

In Figure 11, AOA estimation for the same maneuver as Figure 10 is shown. Since AOA is non-zero for a straight and level flight, the parameters for $C_{z\alpha}$ are made observable, resulting in an accurate approximation. A bias is visible between the data sets, which is likely due to error in the estimation of wind.

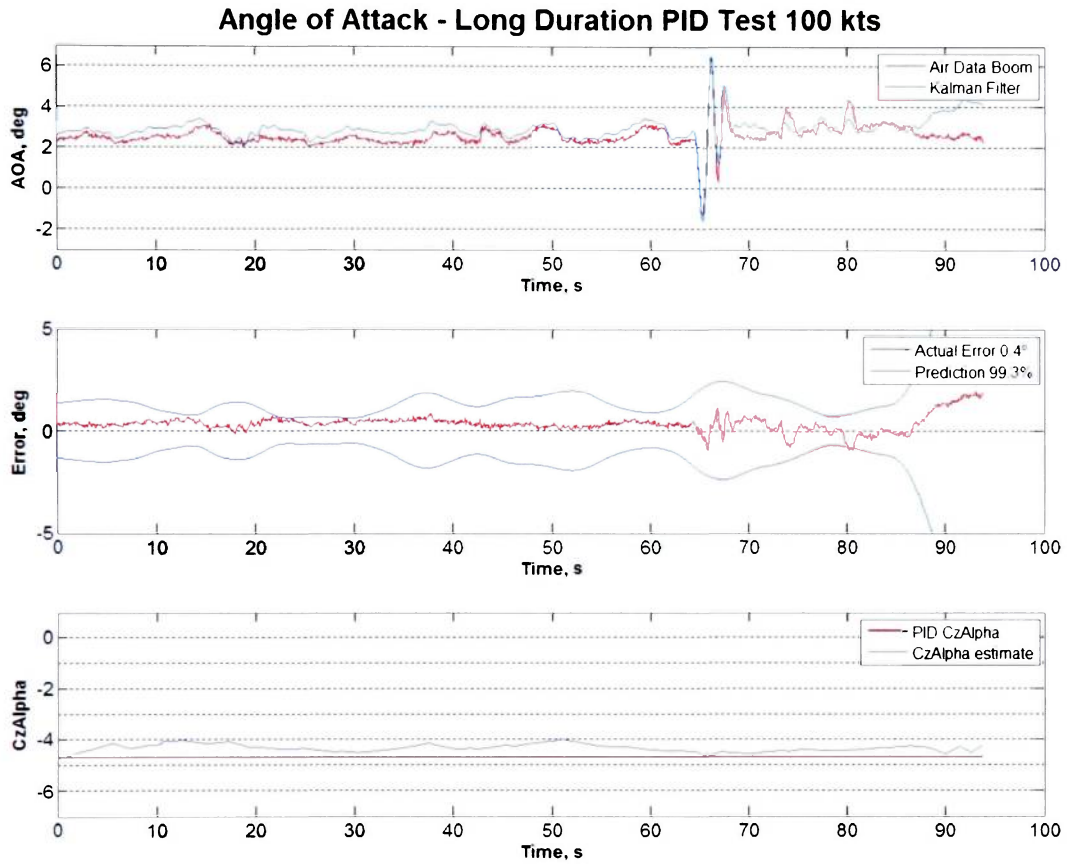


Figure 11: AOA Long Duration PID Test 100 kts (2c6a1100all.csv)

This test is named pseudo long duration because the first 60 seconds of steady state data were copied from the beginning of the file and pasted after the PID maneuver to give a simulated long-duration steady state, both before and after the PID maneuver. This is useful because it shows that the filter will hold a convergence and it makes the convergence of the filter more obvious once the PID maneuver is executed. Once again, this is due to the excitation of the estimated parameters which makes them observable to the Kalman filter so that it can properly converge to a solution for these parameters.

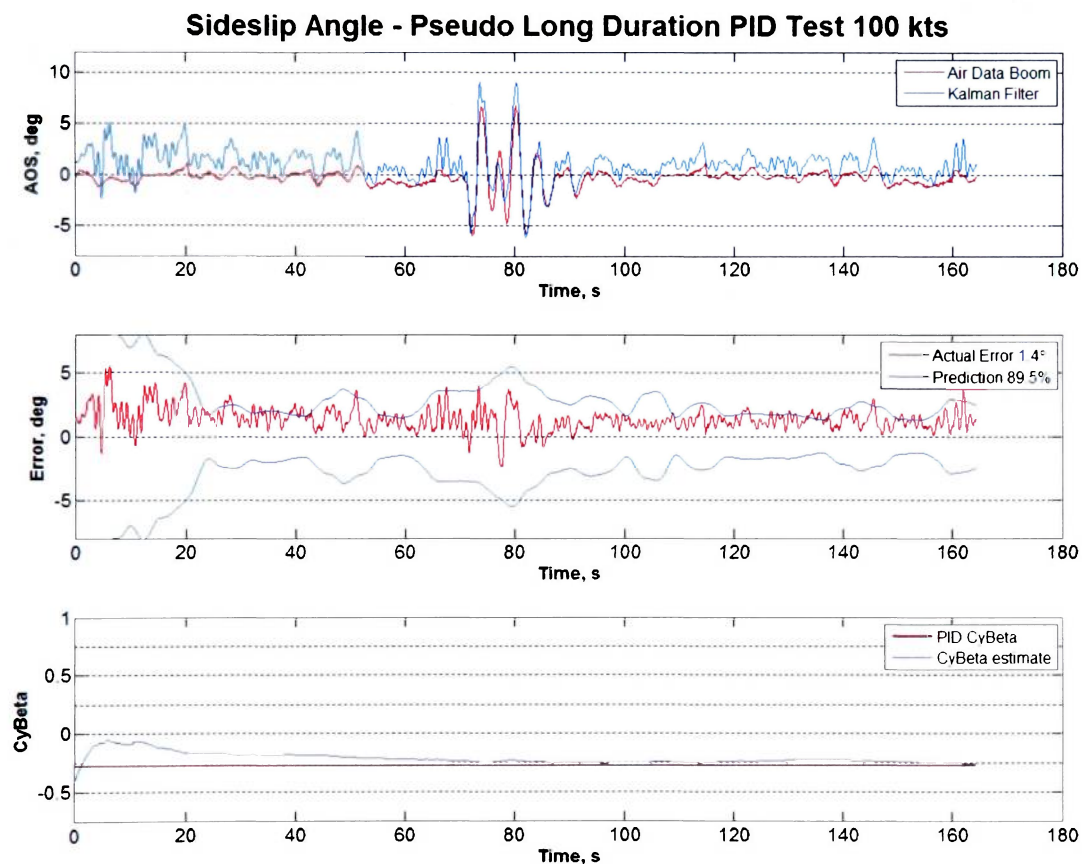


Figure 12: AOS Pseudo Long Duration PID Test 100 kts (2c6a1100all2.csv)

AOA for this pseudo long duration test serves to show the accurate estimation of AOA throughout the steady state periods of the test. Once again, a bias is seen throughout this test, likely due to error in wind estimation. At approximately 90 seconds, a spike in predicted error is seen; this is almost certainly due to a discontinuity in the data from where the first half of this test was copied and appended to the end to simulate a longer test time.

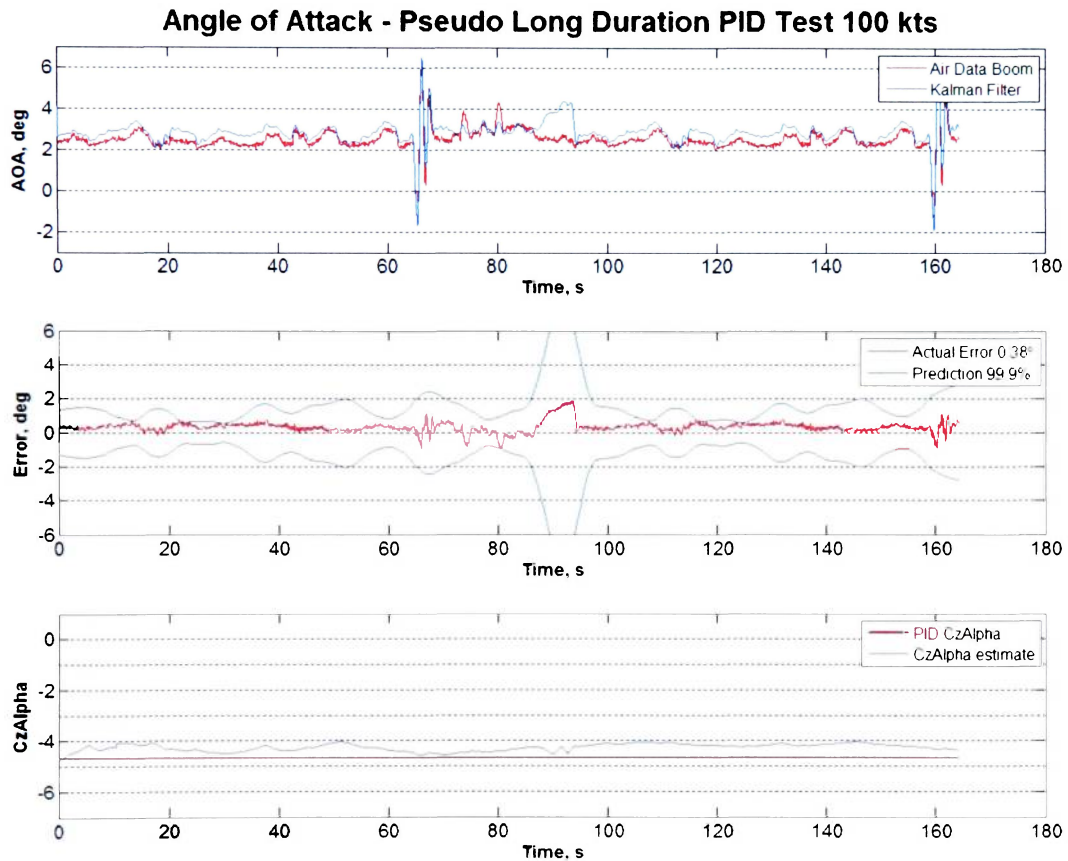


Figure 13: AOA Pseudo Long Duration PID Test 100 kts (2c6a1100all2.csv)

This example is the same data from the previous examples of 100 kts, but without the steady state periods of flight. The estimate of $C_{y\beta}$ converges well to the accepted value once AOS has been made visible.

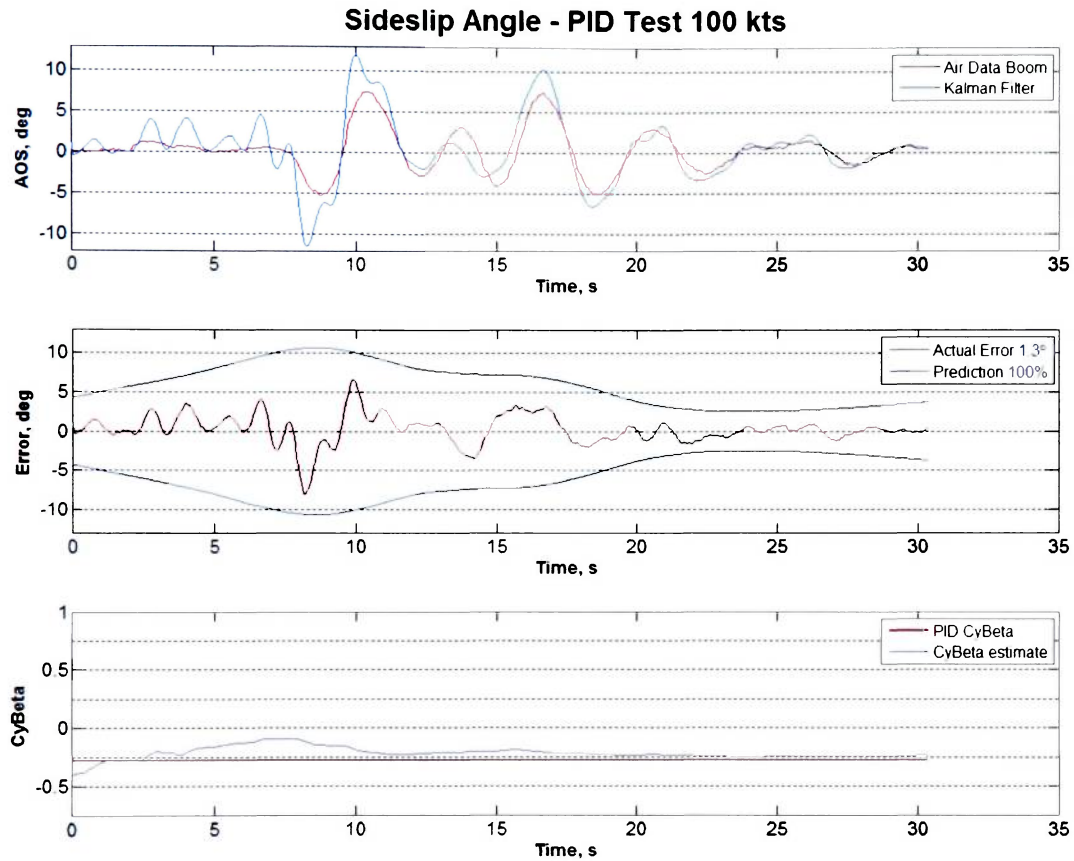


Figure 14: AOS PID Test 100 kts (2c6a1100pid.csv)

The AOA estimate for this test begins well, but loses accuracy over time due to little visibility of the necessary stability derivative, $C_{z\alpha}$. This can be seen by a changing estimate of $C_{z\alpha}$ near the end of the test. A note of inaccuracy of the air data boom is seen at approximately 11 seconds and 17 seconds. The bumps in AOA correspond to positive AOS, likely caused by the alpha vane being disturbed from the airflow coming at it from the side.

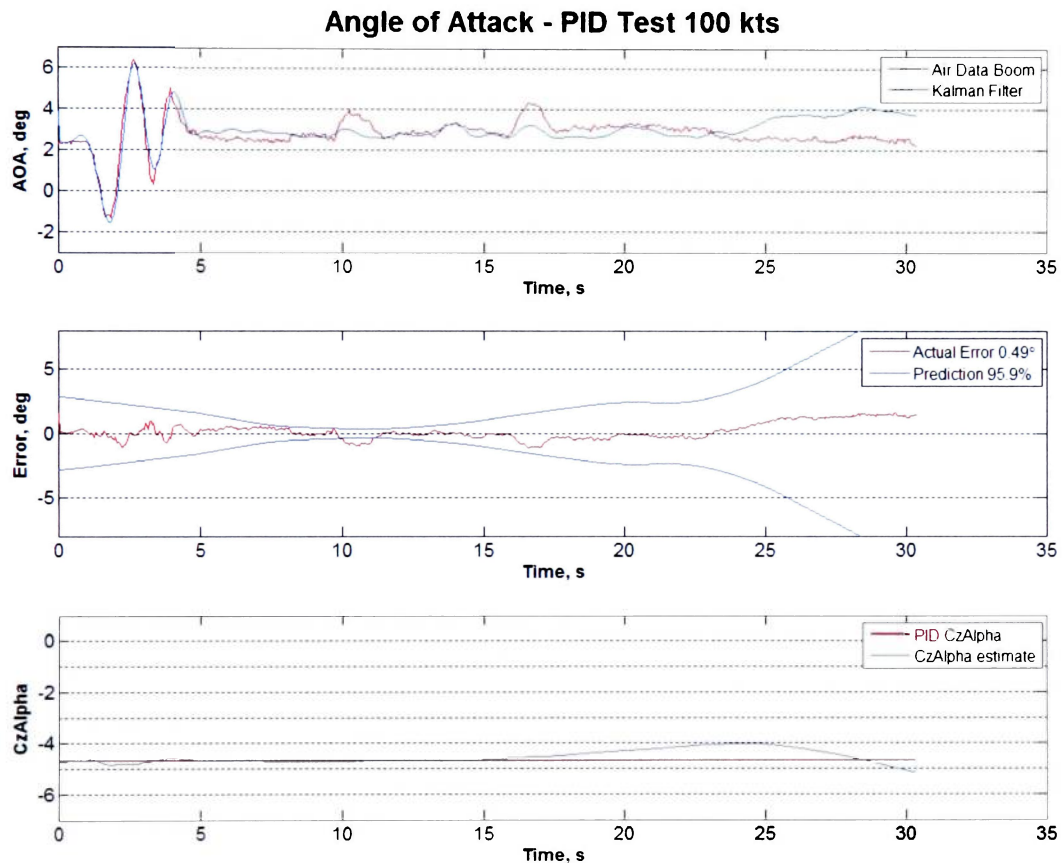


Figure 15: AOA PID Test 100 kts (2c6a1100pid.csv)

This test shows similar results to the previous test, but at a higher initial speed of 120 kts. The AOS estimate converges, which can be seen by the decreasing predicted error and by convergence of $C_{y\beta}$ to the accepted value from previous research.¹⁰ Once again, the method settles on the accepted value even with a shorter test of this type.

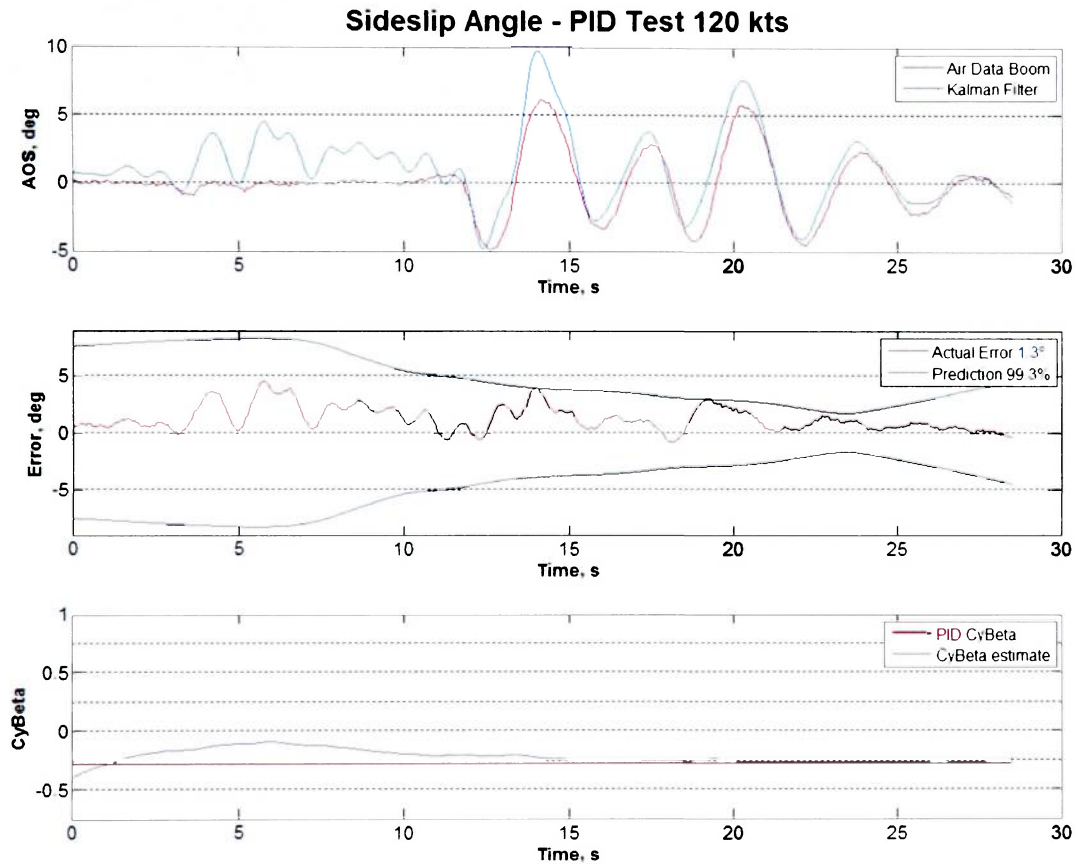


Figure 16: AOS PID Test 120 kts (2c6a1120pid.csv)

In the following figure, after alpha is made visible with the pitch maneuver, it has a good approximation, but loses accuracy over time due to little alpha visibility. Note that the AOA bumps at approx 15 secs and 20 secs from the air data boom correspond with large positive changes in AOS.

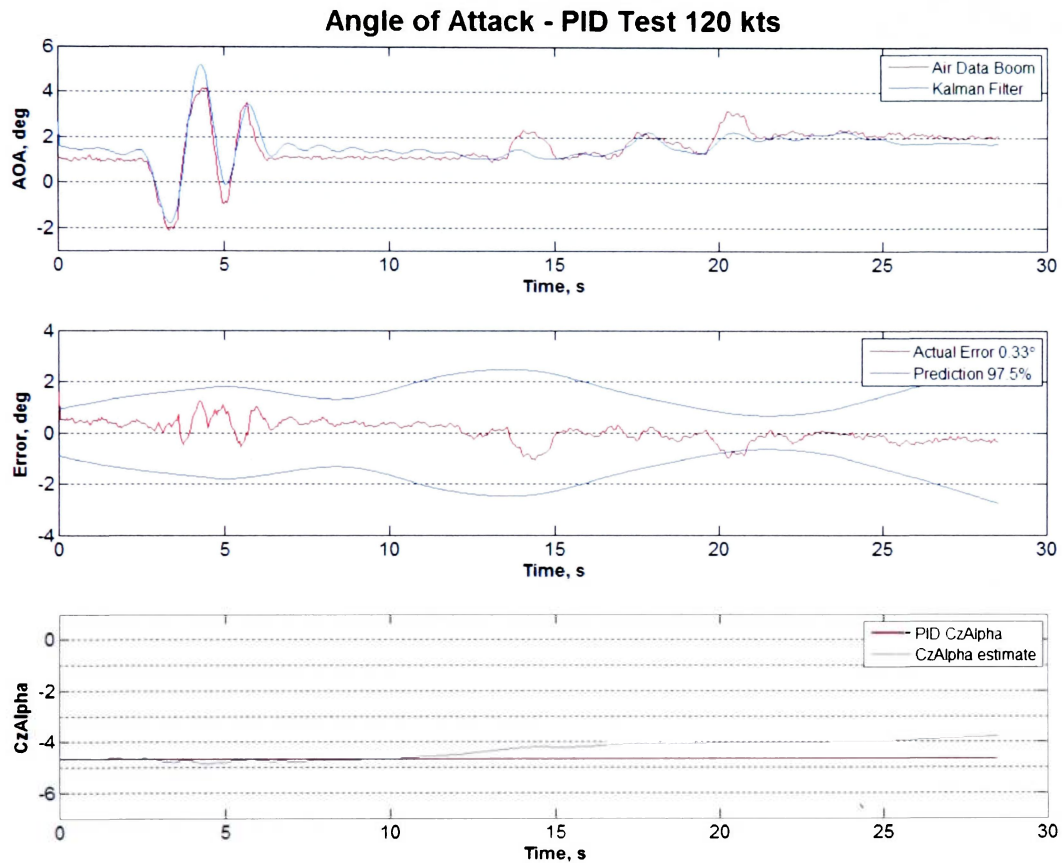


Figure 17: AOA PID Test 120 kts (2c6a1120pid.csv)

The following example of a PID test starting at 75 kts shows a quicker convergence than previous examples. Another note is that the INS data may have lagged at approximately 30 seconds.

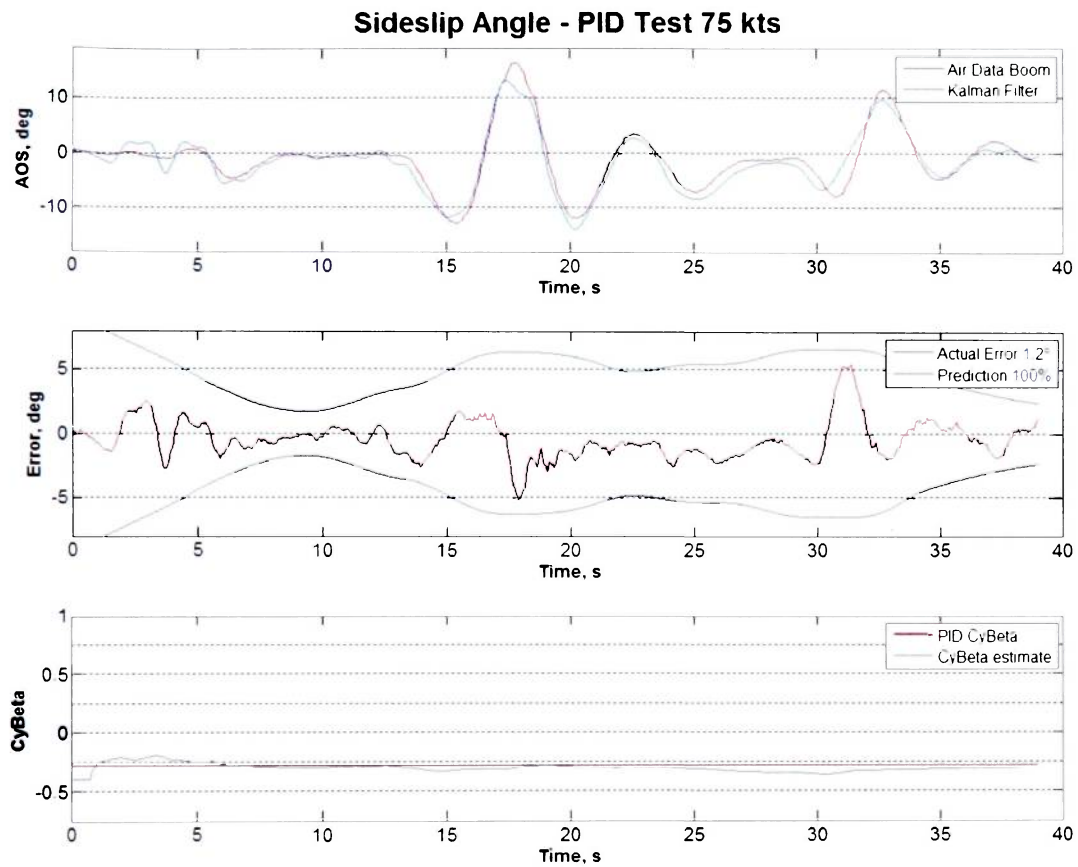


Figure 18: AOS PID Test 75 kts (2c6a175pid.csv)

Alpha is visible with the pitch maneuver and has a good approximation, but loses accuracy rapidly due to an unknown anomaly. It is possible that the lack of stability derivative visibility causes the drastic shift in $C_{z\alpha}$.

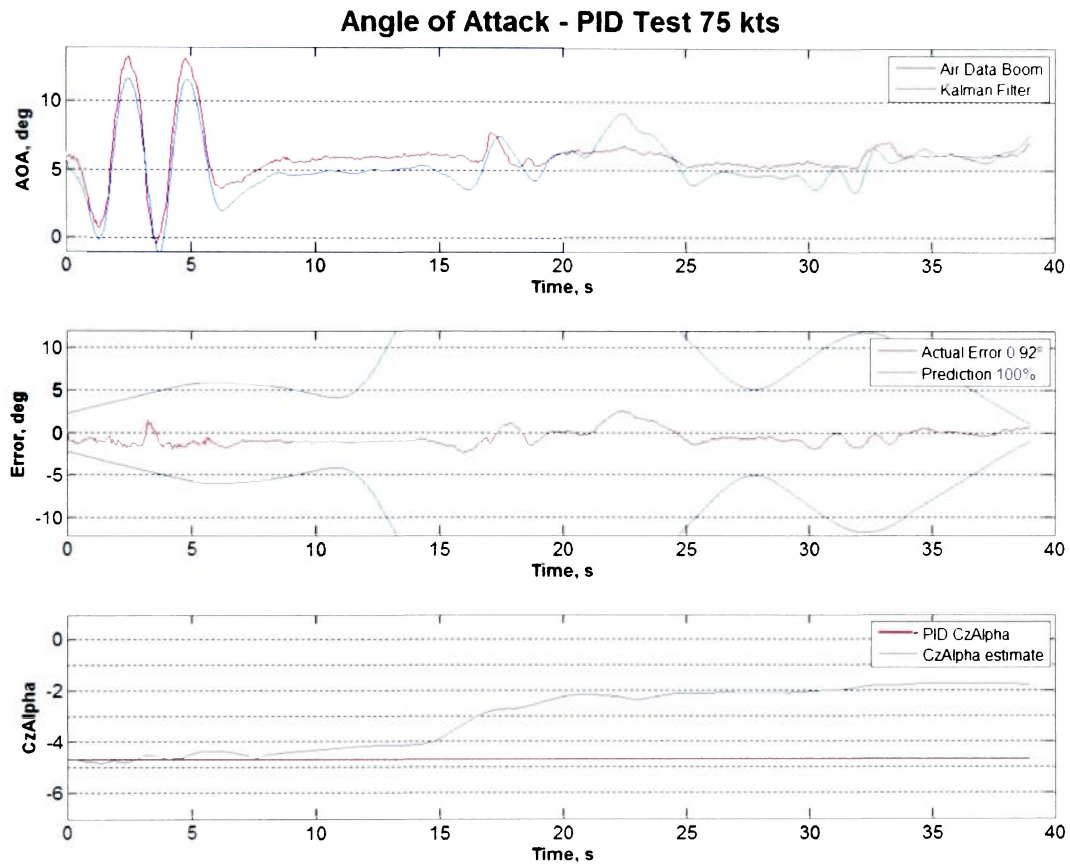


Figure 19: AOA PID Test 75 kts (2c6a175pid.csv)

This example is from a test performed at 145 kts, and shows similar results to the other PID tests. This test seems to show a small bias in the INS data, but still shows good convergence for $C_{y\beta}$.

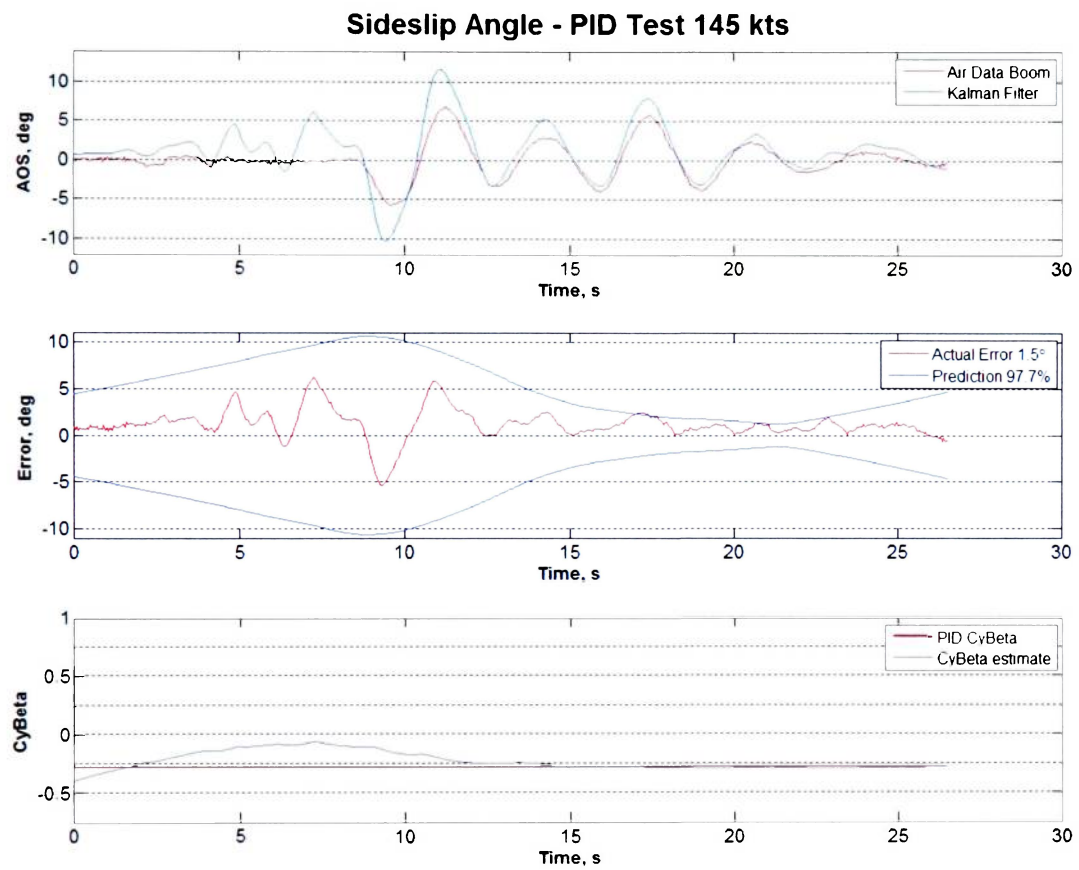


Figure 20: AOS PID Test 145 kts (2c6a1maxpid.csv)

This test shows an accurate AOA estimate with little to no bias, likely due to a successful estimation of the wind with the AGARD method. $C_{z\alpha}$ is seen at the correct value, but begins to drift as time continues without making angle of attack visible.

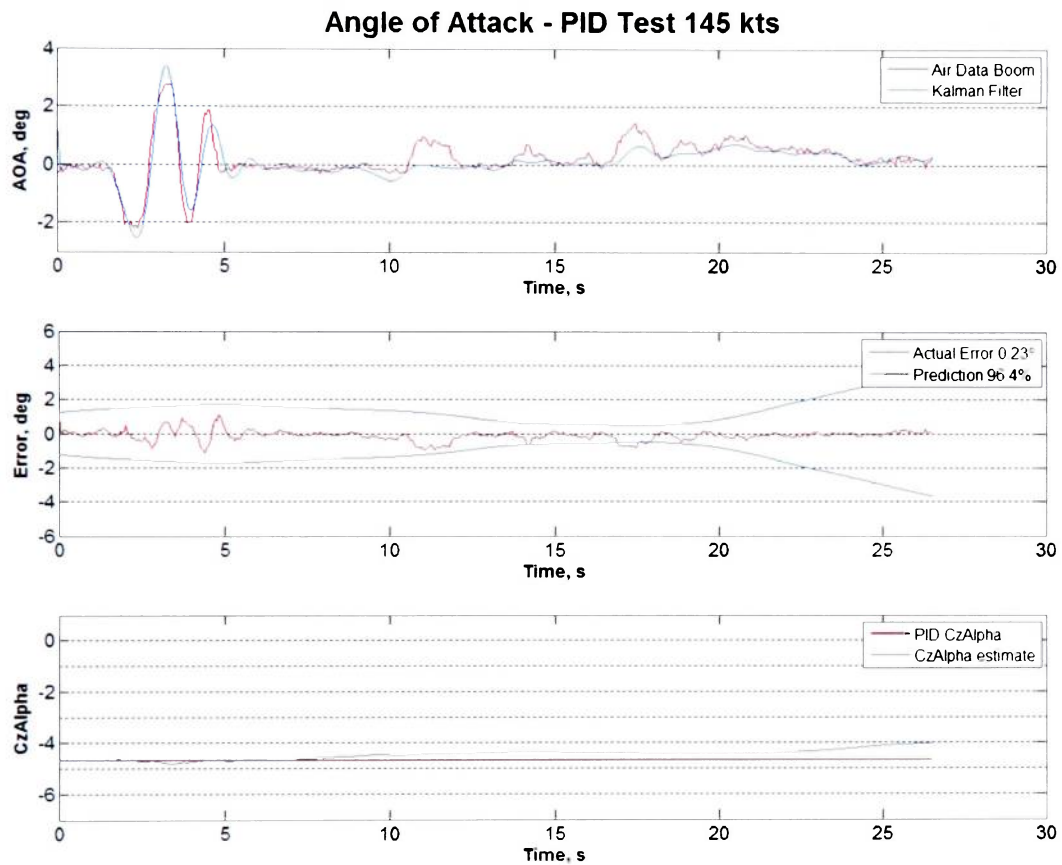


Figure 21: AOA PID Test 145 kts (2c6a1maxpid.csv)

This case is the first example in which the Kalman filter was unable to converge. As is shown, the motion in this test is primarily longitudinal, leaving the lateral/directional motion negligible. Since not enough motion is seen on the lateral/direction axes, the filter is unable to converge to an accurate solution. Simultaneously, the predicted error is off scale due to the non-convergence of the filter in this scenario. In this case, the predicted error is primarily driven by the Kalman covariance parameter. This example is useful to show the requirement of making the necessary parameters observable by aircraft motion.

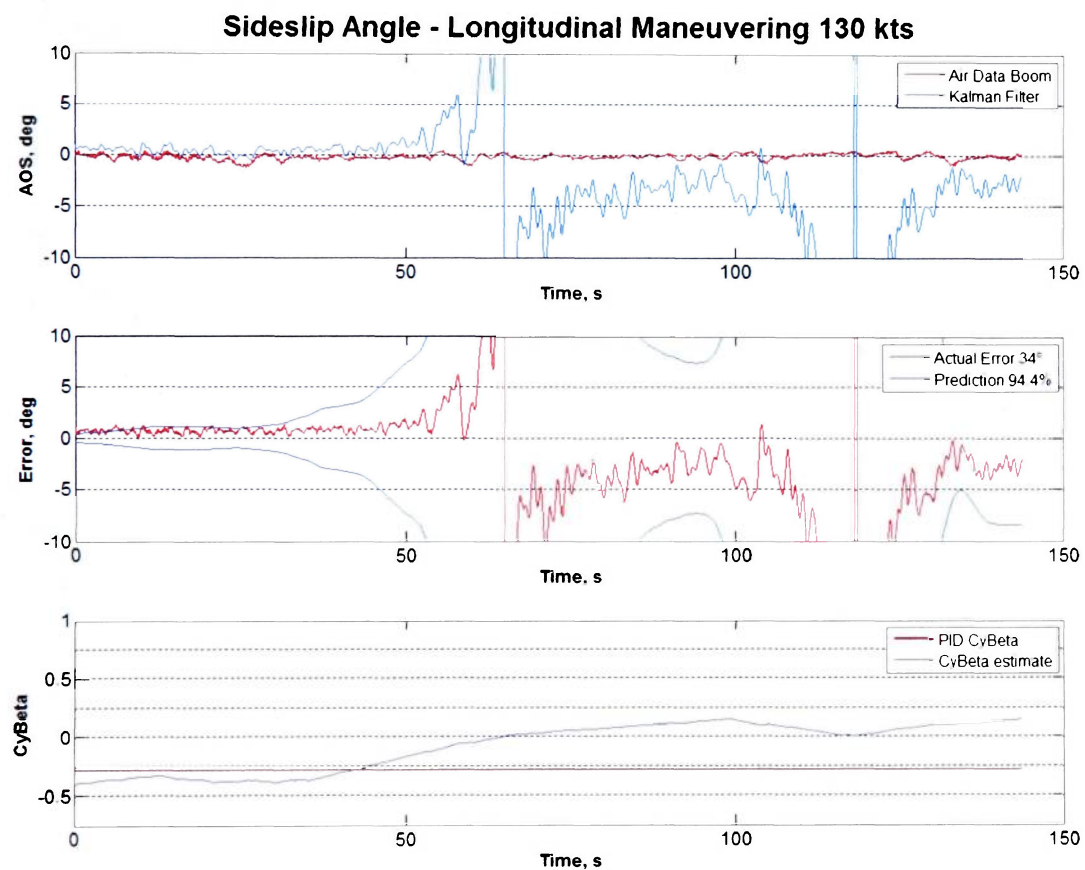


Figure 22: AOS Longitudinal Maneuvering 130 kts (2c7a1.csv)

Although AOA in this test does not go through periods of rapid change such as in the PID maneuvers, it is always a non-zero value, which allows the filter method to converge and makes the initial AGARD method estimation of AOA more accurate and useful. Accuracy is lost near the end of this case due to an oscillation in the estimation of $C_{z\alpha}$ due to lack of dynamics. .

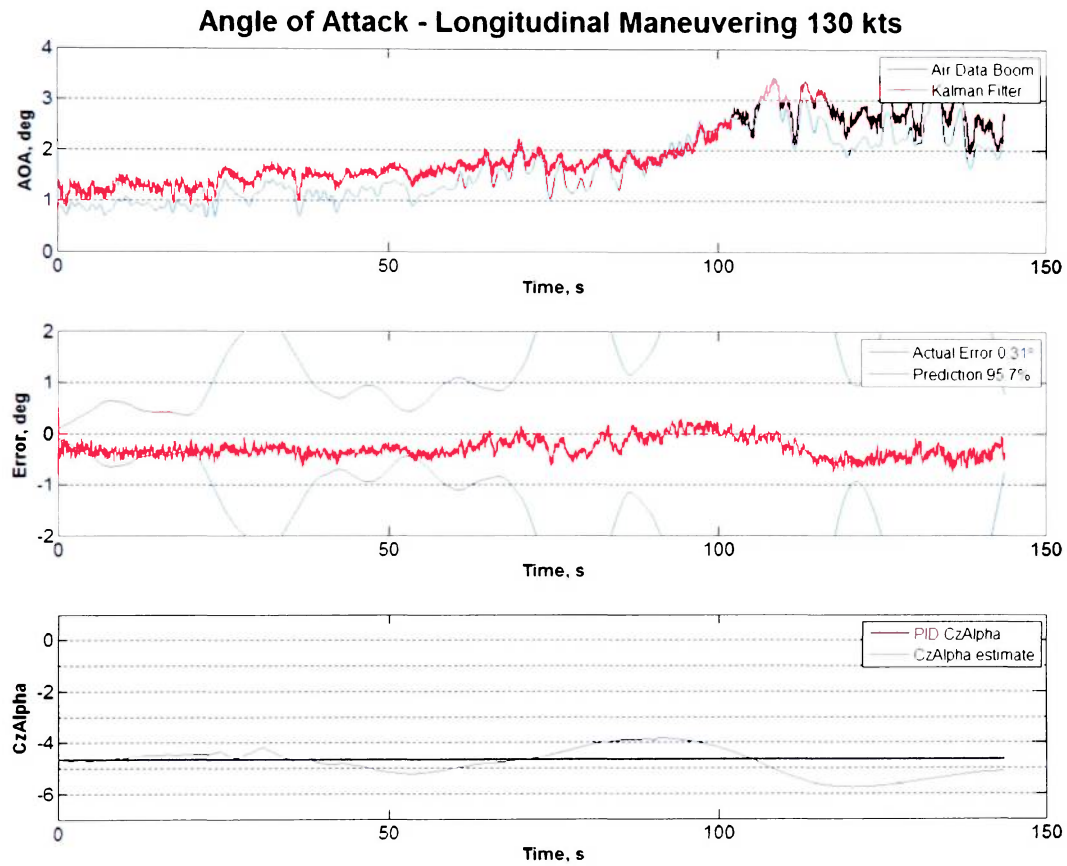


Figure 23: AOA Longitudinal Maneuvering 130 kts (2c7a1.csv)

The next example shows repeated Dutch roll maneuvers, which constantly make AOS observable resulting in good convergence and an accurate estimation for $C_{y\beta}$.

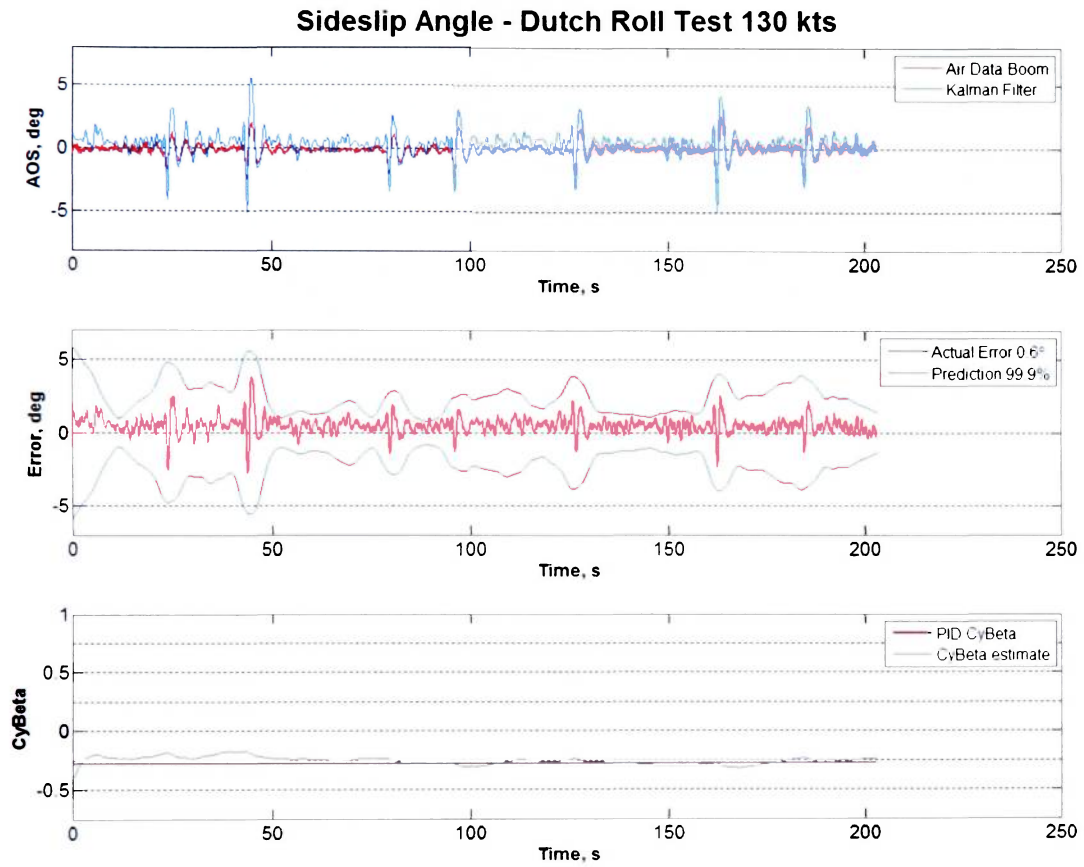


Figure 24: AOS Dutch Roll Test 130 kts (2d7a1.csv)

In this case, the AOA estimate loses accuracy because minimal longitudinal dynamics are seen; without a maneuver similar to PID, the filter is unable to observe the stability derivatives and diverges when estimating $C_{z\alpha}$. This test only excites the lateral/direction axes and is not normally interesting in the longitudinal axis.

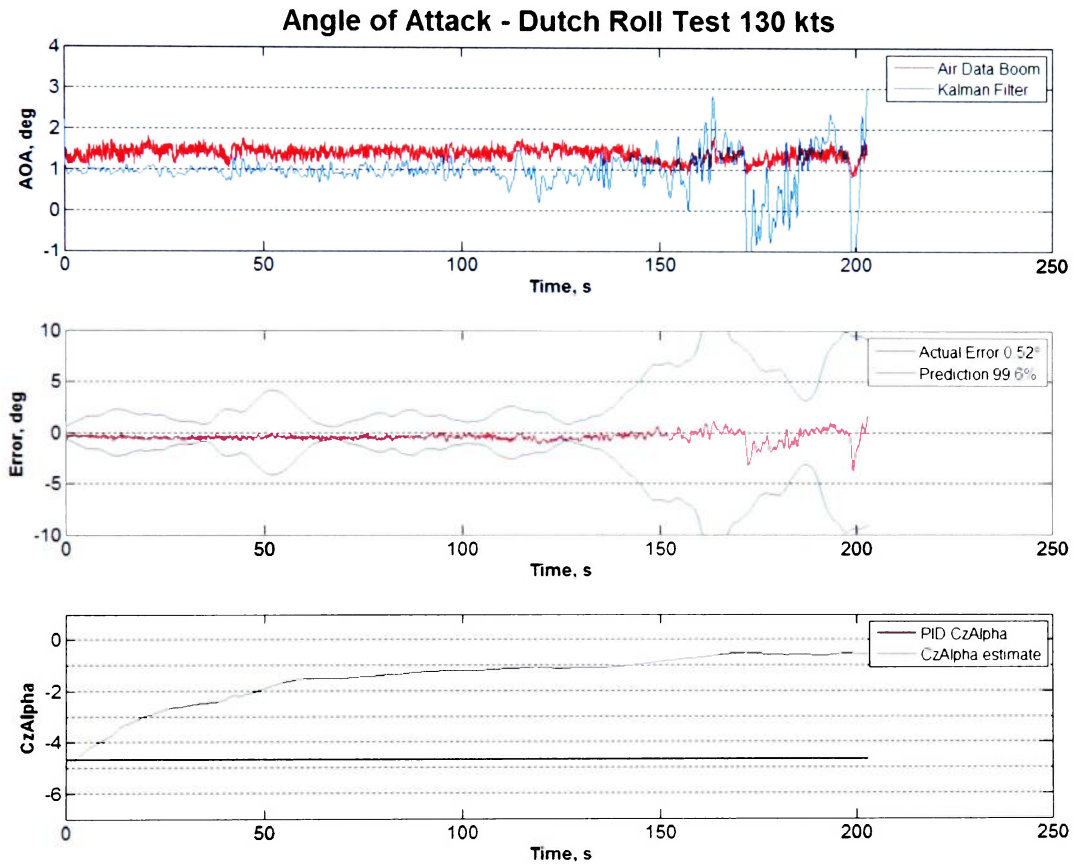


Figure 25: AOA Dutch Roll Test 130 kts (2d7a1.csv)

In the following figure, steady state sideslip shows relatively high accuracy when measuring AOS. This method seems to work the best with steady heading sideslip cases likely due to the consistent AOS observability. It should be noted that this test originally had a user input data error for the aircraft fuel, resulting in a drastically inaccurate estimate of the aircraft weight. This incorrect weight caused the filter to converge to a significantly different value for $C_{y\beta}$, but has since been corrected for.

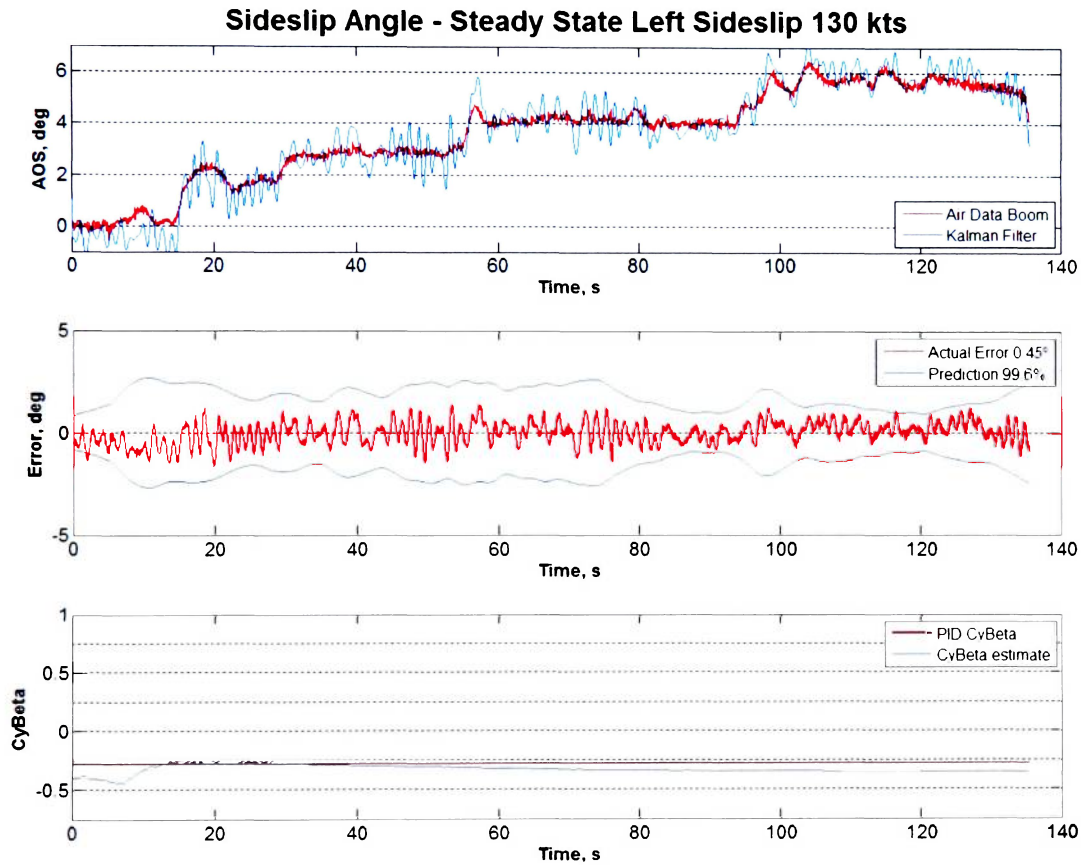


Figure 26: AOS Steady State Left Sideslip 130 kts (2d8al-correct-weight.csv)

In this case, the AOA estimate loses accuracy because minimal longitudinal dynamics are seen; without a maneuver similar to PID, the filter is unable to observe the stability derivatives and diverges when estimating $C_{z\alpha}$. This test only excites the lateral/direction axes and is not normally interesting in the longitudinal axis.

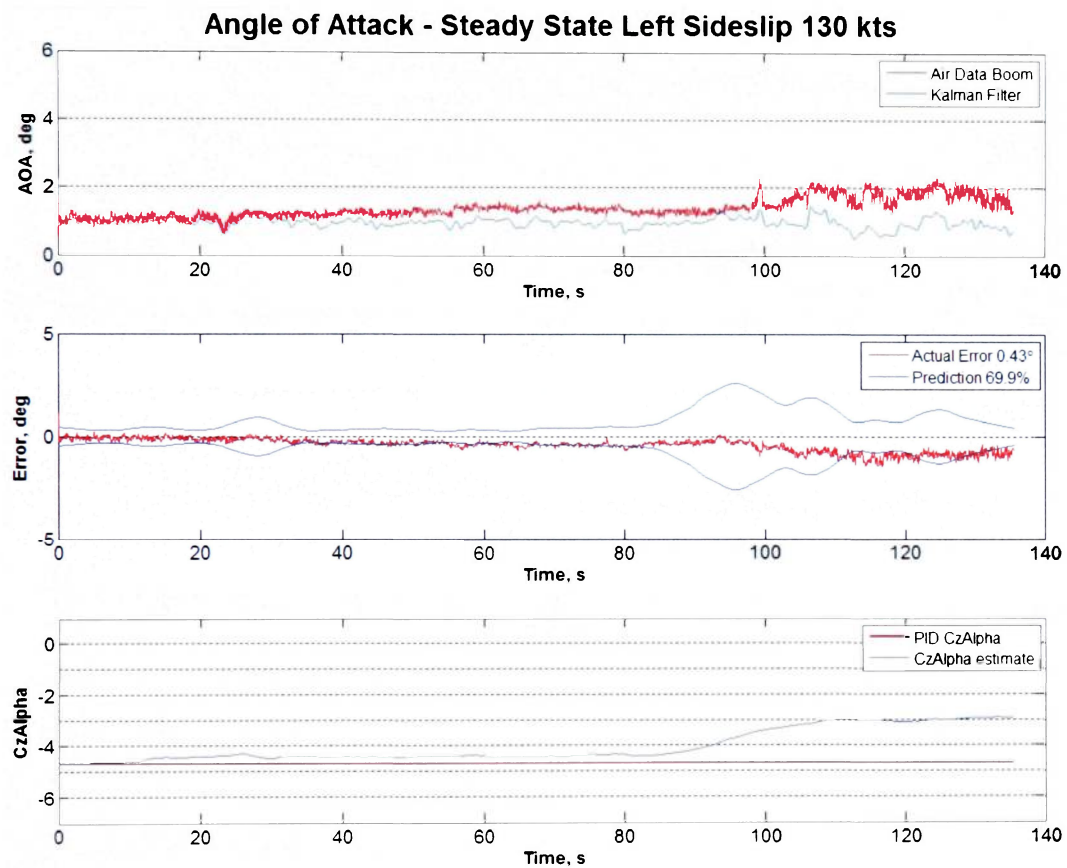


Figure 27: AOA Steady State Left Sideslip 130 kts (2d8al-correct-weight.csv)

This is another example of accurate estimation of AOS during a steady state sideslip test. Accuracy is roughly equal to the previous steady heading sideslip example, but the converged value for $C_{y\beta}$ is significantly different due to this case being in the gear-down configuration. This case also shows a sideslip from the right compared to the previous case from the left; no difference is noticed in accuracy between left or right sideslip.

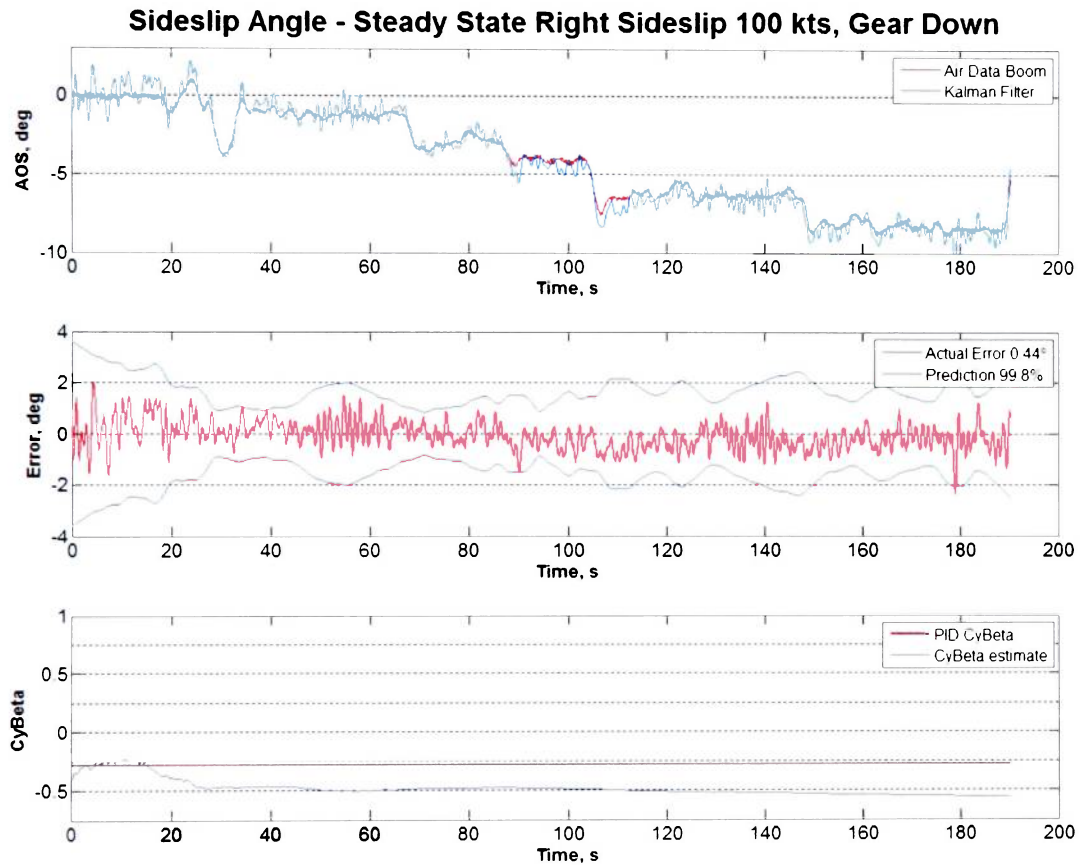


Figure 28: AOS Steady State Right Sideslip 100 kts, Gear Down (2d8br.csv)

In this case, the AOA estimate loses accuracy because minimal longitudinal dynamics are seen; without a maneuver similar to PID, the filter is unable to observe the stability derivatives and diverges when estimating $C_{z\alpha}$. This test only excites the lateral/direction axes and is not normally interesting in the longitudinal axis.

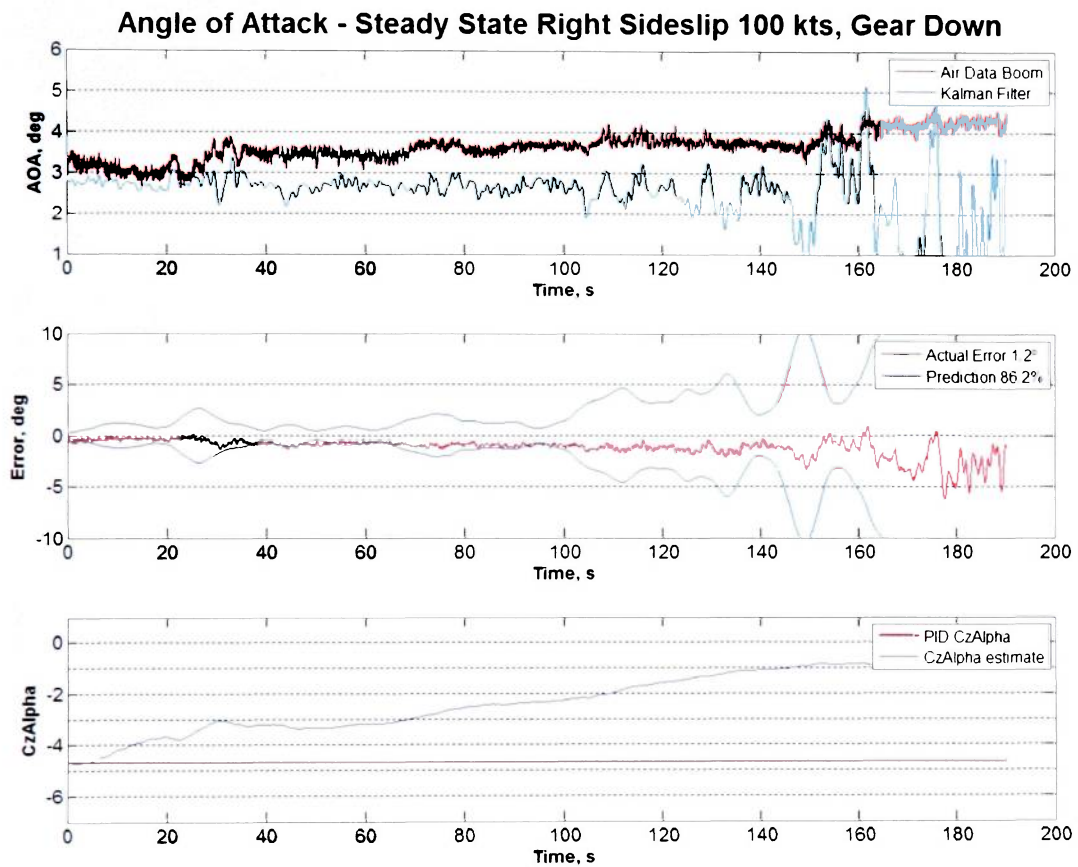


Figure 29: AOA Steady State Right Sideslip 100 kts, Gear Down (2d8br.csv)

The next figure confirms that another gear-down case converges to the same value for $C_{y\beta}$ as the other gear-down case, and continues to maintain an accurate estimation.

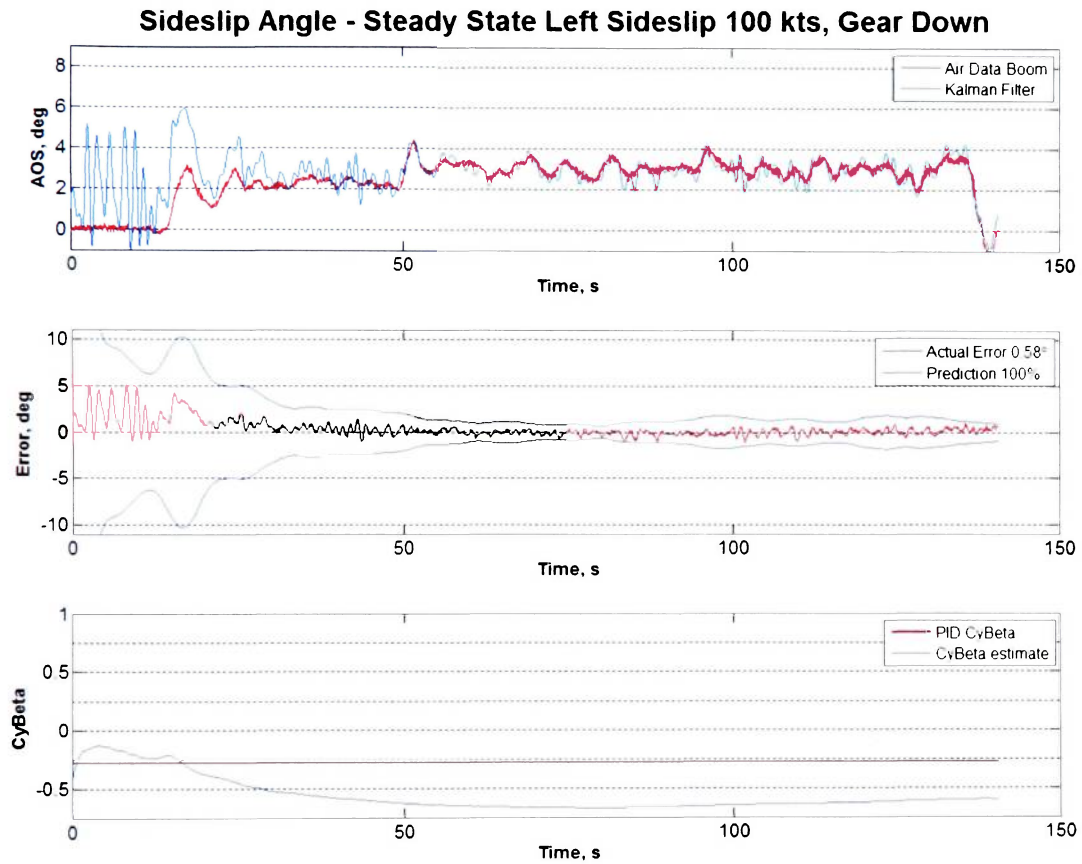


Figure 30: AOS Steady State Left Sideslip 100 kts, Gear Down (2d8bl.csv)

In this case, the AOA estimate loses accuracy because minimal longitudinal dynamics are seen; without a maneuver similar to PID, the filter is unable to observe the stability derivatives and diverges when estimating $C_{z\alpha}$. This test only excites the lateral/direction axes and is not normally interesting in the longitudinal axis.

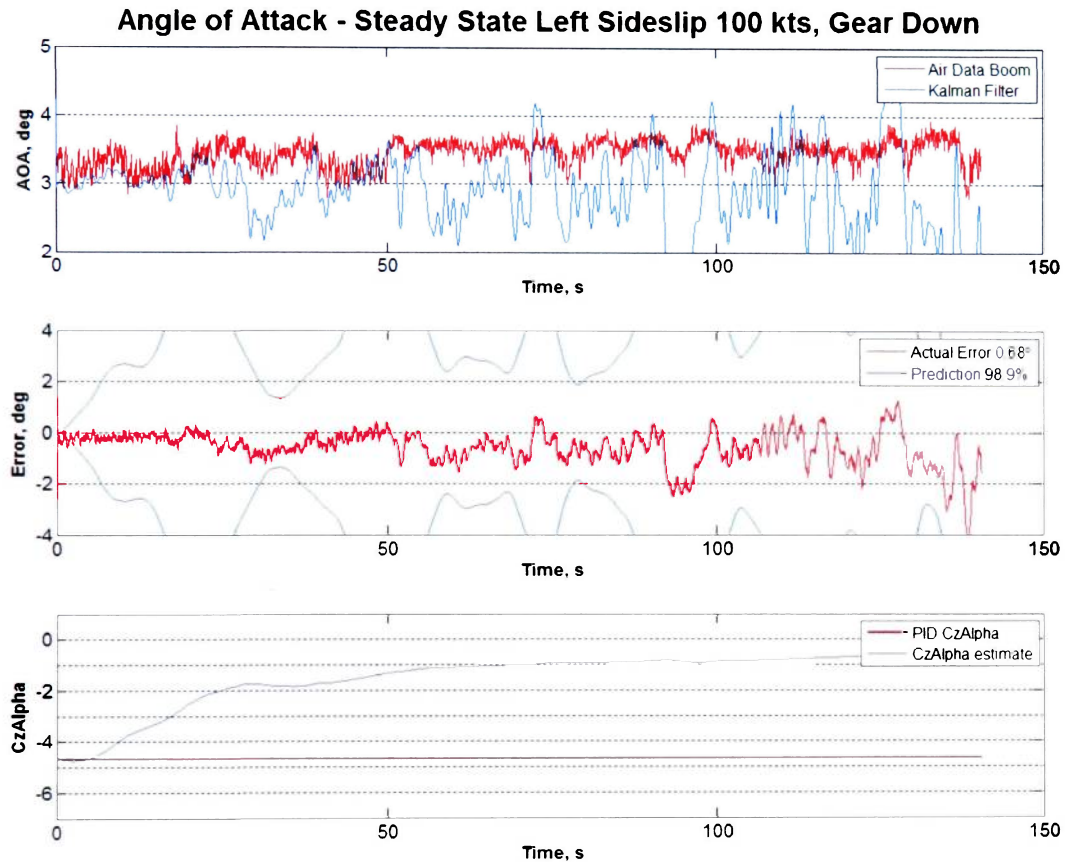


Figure 31: AOA Steady State Left Sideslip 100 kts, Gear Down (2d8bl.csv)

The next figure confirms that another gear-down case converges to the same value for $C_{y\beta}$ as the other gear-down cases, and continues to maintain an accurate estimation. This case also has 50% flaps down, which has a negligible effect on $C_{y\beta}$.

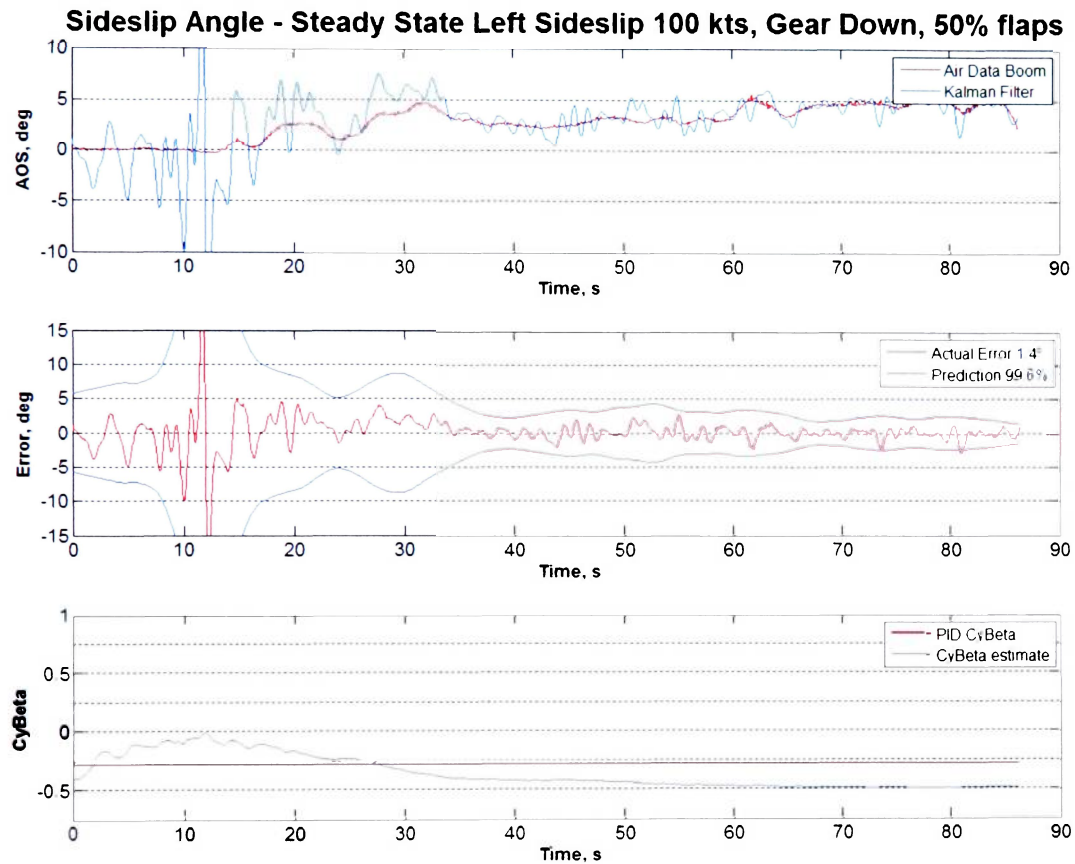


Figure 32: AOS Steady State Left Sideslip 100 kts, Gear Down, 50% flaps (2d8cl.csv)

In this case, the AOA estimate loses accuracy because minimal longitudinal dynamics are seen; without a maneuver similar to PID, the filter is unable to observe the stability derivatives and diverges when estimating $C_{z\alpha}$. This test only excites the lateral/direction axes and is not normally interesting in the longitudinal axis.

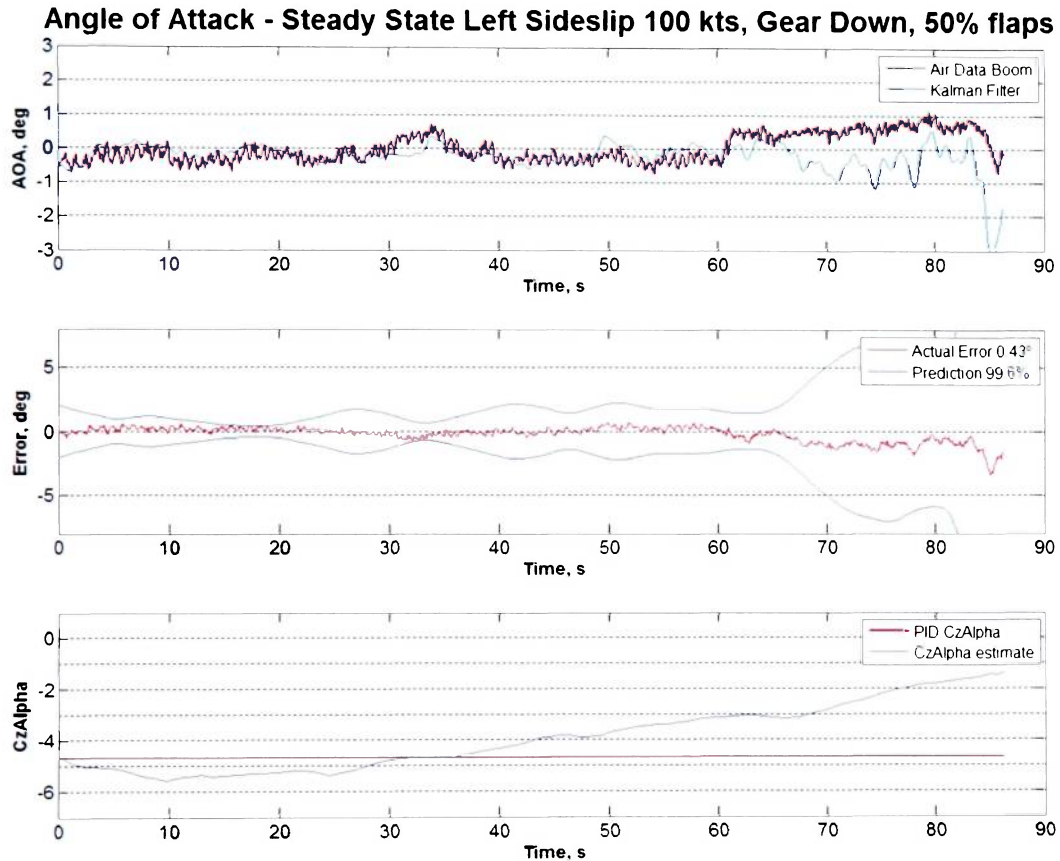


Figure 33: AOA Steady State Left Sideslip 100 kts, Gear Down, 50% flaps (2d8cl.csv)

The next figure confirms that another gear-down case converges to the same value for $C_{y\beta}$ as the other gear-down cases, and continues to maintain an accurate estimation. This case also has 50% flaps down which has a negligible effect for $C_{y\beta}$.

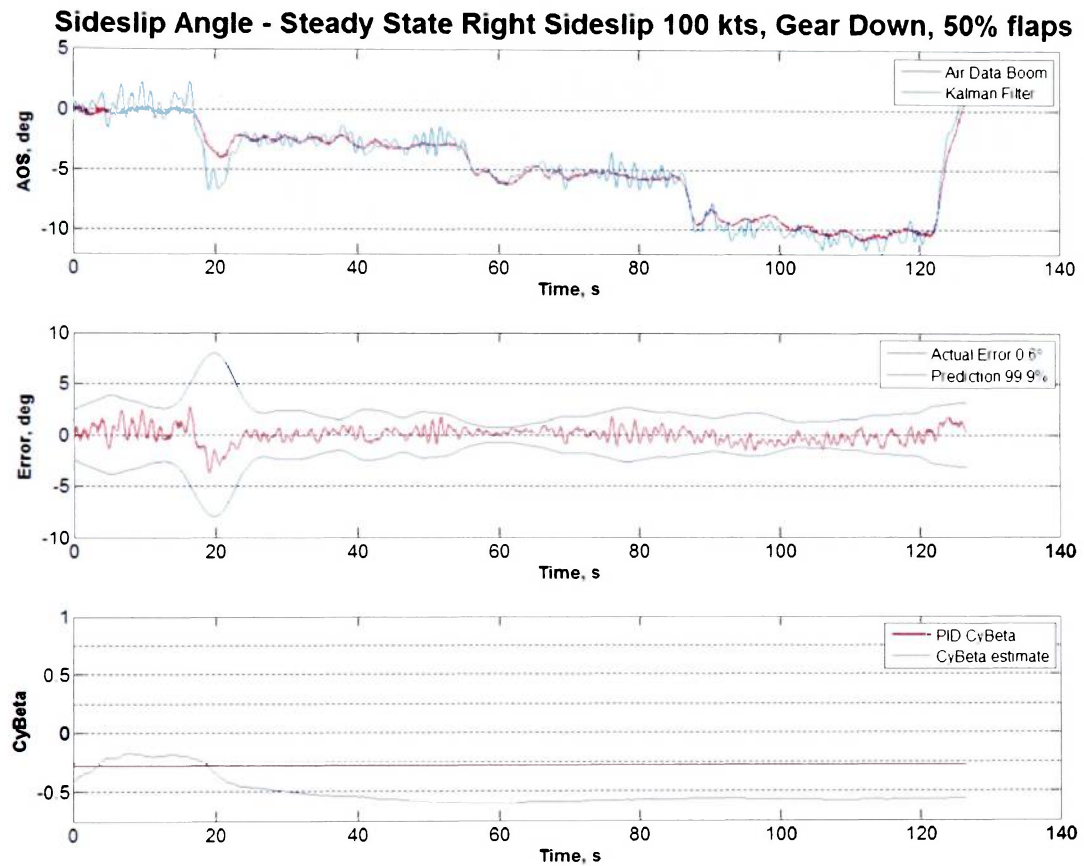


Figure 34: AOS Steady State Right Sideslip 100 kts, Gear Down, 50% flaps (2d8cr.csv)

In this case, the AOA estimate loses accuracy because minimal longitudinal dynamics are seen; without a maneuver similar to PID, the filter is unable to observe the stability derivatives and diverges when estimating $C_{z\alpha}$. This test only excites the lateral/direction axes and is not normally interesting in the longitudinal axis.

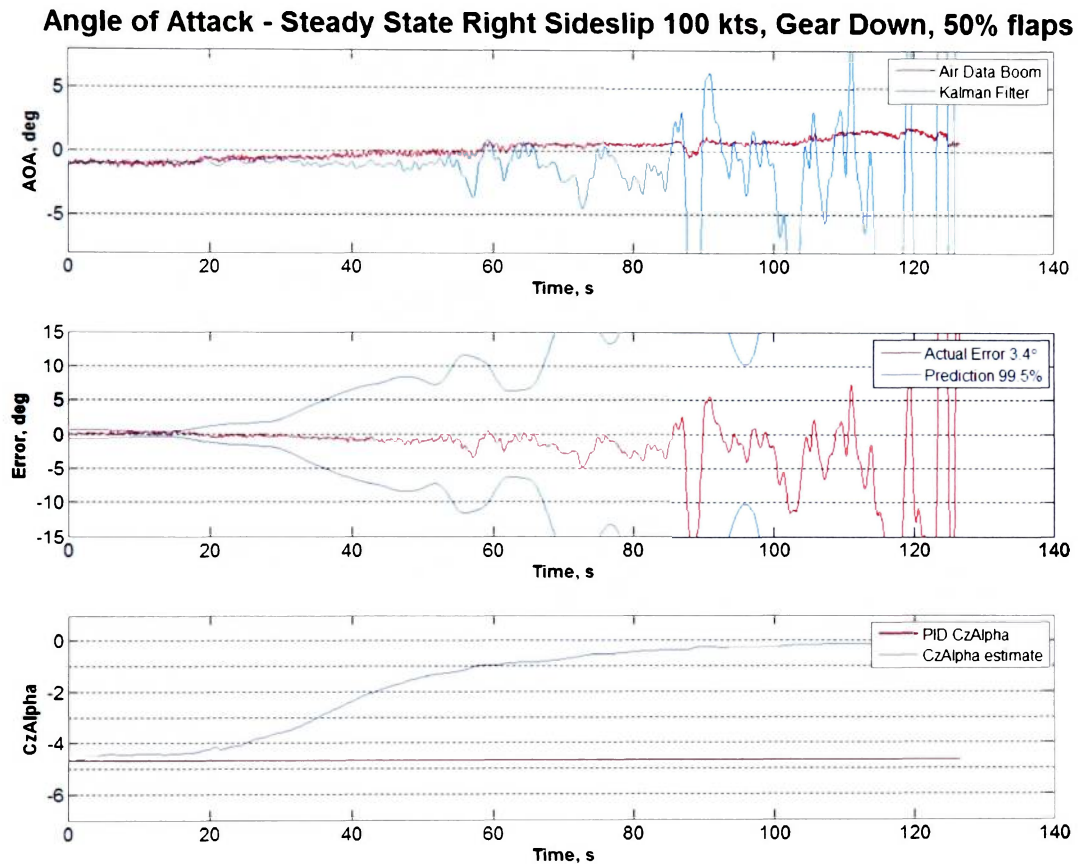


Figure 35: AOA Steady State Right Sideslip 100 kts, Gear Down, 50% flaps (2d8cr.csv)

4. CONCLUSIONS

The purpose of this study was to explore the use of INS systems as a primary method for measuring aircraft air flow angles in flight testing. The idea behind this is that this method could be used as an alternative to the traditional methods for measuring aircraft air flow angles but, before doing so, it must be shown to be accurate enough to be used in place of the traditional methods.

Figure	Title	Maneuver Axis	Speed	Gear/Flaps	$C_{y\beta}$	Predicted Error Confidence	Mean Error in β
10	Long Duration PID	Lat /Dir + Long	100 kts	Up/0°	-0.23	92.1%	1.7°
12	Pseudo Long Duration PID	Lat /Dir + Long	100 kts	Up/0°	-0.26	89.5%	1.4°
14	PID	Lat /Dir + Long	100 kts	Up/0°	-0.24	100%	1.3°
16	PID	Lat /Dir + Long	120 kts	Up/0°	-0.25	99.3%	1.3°
18	PID	Lat /Dir + Long	75 kts	Up/0°	-0.3	100%	1.2°
20	PID	Lat /Dir + Long	145 kts	Up/0°	-0.28	97.7%	1.5°
22	Longitudinal Maneuvering	Longitudinal	130 kts	Up/0°	0.14	94.4%	34°
24	Dutch Roll	Lateral/Directional	130 kts	Up/0°	-0.24	99.9%	0.6°
26	Steady State Left Sideslip	Lateral/Directional	130 kts	Up/0°	-0.33	99.6%	0.45°
28	Steady State Right Sideslip	Lateral/Directional	100 kts	Down/0°	-0.6	99.8%	0.44°
30	Steady State Left Sideslip	Lateral/Directional	100 kts	Down/0°	-0.56	100%	0.58°
32	Steady State Left Sideslip	Lateral/Directional	100 kts	Down/50°	-0.49	99.6%	1.4°
34	Steady State Right Sideslip	Lateral/Directional	100 kts	Down/50°	-0.57	99.9%	0.6°

Compilation of Sideslip Angle Results

In review of the table of sideslip angle results above, a few observations should be noted. Test maneuvers that involve the lateral and directional axes have significantly lower error than maneuvers that are solely in the longitudinal axis. This is expected, as dynamics on the lateral/directional axes are necessary to make $C_{y\beta}$ visible for the filter to converge. Also, tests involving only lateral and directional axes, with little dynamics on the longitudinal axis, have even lower error than maneuvers involving all three axes. Estimates for $C_{y\beta}$ are fairly constant throughout, but seem to depend slightly on the maneuver. It also stands out that estimates for $C_{y\beta}$ change significantly for tests in the gear down

configuration. This is expected, because with the gear in the down position, the lateral surface of the aircraft has changed significantly.

Figure	Title	Maneuver Axis	Speed	Gear/Flaps	$C_{z\alpha}$	Predicted Error Confidence	Mean Error in α
11	Long Duration PID	Lat /Dir + Long	100 kts	Up/0°	-4.3	99.3%	0.4°
13	Pseudo Long Duration PID	Lat /Dir + Long	100 kts	Up/0°	-4.4	99.9%	0.38°
15	PID	Lat /Dir + Long	100 kts	Up/0°	-4.7	95.9%	0.49°
17	PID	Lat /Dir + Long	120 kts	Up/0°	-4.7	97.5%	0.33°
19	PID	Lat /Dir + Long	75 kts	Up/0°	-4.5	100%	0.92°
21	PID	Lat /Dir + Long	145 kts	Up/0°	-4.8	96.4%	0.23°
23	Longitudinal Maneuvering	Longitudinal	130 kts	Up/0°	-4.9	95.7%	0.31°
25	Dutch Roll	Lateral/Directional	130 kts	Up/0°	-0.59	99.6%	0.52°
27	Steady State Left Sideslip	Lateral/Directional	130 kts	Up/0°	-3.5	69.9%	0.43°
29	Steady State Right Sideslip	Lateral/Directional	100 kts	Down/0°	-0.66	86.2%	1.2°
31	Steady State Left Sideslip	Lateral/Directional	100 kts	Down/0°	-0.26	98.9%	0.68°
33	Steady State Left Sideslip	Lateral/Directional	100 kts	Down/50°	-1.4	99.6%	0.43°
35	Steady State Right Sideslip	Lateral/Directional	100 kts	Down/50°	-0.05	99.5%	3.4°

Compilation of Angle of Attack Results

The table above presents a few observations about the angle of attack estimation. It is made quite obvious that when estimating $C_{z\alpha}$, maneuvers in the longitudinal axis are necessary. All tests in the longitudinal axis arrive at a similar value for $C_{z\alpha}$ while all maneuvers that are only in the lateral and directional axes have drastically poor estimations.

4.1 Parameter Identification

The accuracy of this method is driven directly by the accuracy of the estimation of the aircraft's stability derivatives, specifically $C_{y\beta}$ and $C_{z\alpha}$. Many projects are available which study the accuracy of stability derivative estimation and, more recently, real-time parameter identification. The methods employed to estimate these stability derivatives for this thesis are a unique subset of real-time parameter identification. The Kalman filter which attempts to converge to a solution for these stability derivatives is not fully optimized, and is continually being fed more information about the aircraft, which

results in the filter reaching an accurate estimation, but only temporarily. As time passes, the filter receives information where the stability derivatives are unobservable, i.e. the aircraft is not undergoing dynamic maneuvers. This poor information being fed to the filter causes its estimation of the stability derivative to degrade in accuracy, until the proper dynamic maneuvers are performed. Further work would be useful in optimizing the Kalman filter to converge to an accurate solution, and to maintain that solution, even after a long time period of unobservable stability derivatives. The fact that the Kalman filter works well for some periods, while losing accuracy in others, causes the overall accuracy of the method to be highly dependent on the test maneuver being performed. Most tests shown in this report were in the cruise configuration, but basic study has shown this method's accuracy is not significantly dependant on aircraft configuration, airspeed, or altitude.

4.2 Air Flow Angle Accuracy

Estimation of air flow angles for PID maneuvers with this method are characterized by inaccurate AOS estimations until the lateral/directional dynamics of the test are seen; at that point, the accuracy of the method improves, but a more comprehensive analysis would need to be performed to show that this would be sufficient to replace traditional AOS measurement methods. AOA estimation for PID tests is generally on the same level of accuracy as AOS, but sometimes shows a slight bias. PID estimations for AOS are roughly within 1.4 degrees of error and AOA are roughly within 0.5 degrees; both show potential for use as an alternative to traditional air flow angle measurements. More work with the Kalman filter convergence might improve the final solution of this method.

The longitudinal maneuvering test included, serves as an example for when the estimation for AOS does not work well. With no lateral/directional maneuvering in this test, $C_{y\beta}$ is never observable to the Kalman filter; thus, it never converges properly and results in a worthless estimation of AOS. AOA is estimated well, roughly within 0.5 degrees.

Dutch roll tests yield essentially the opposite result of the longitudinal maneuvering test. With frequent Dutch rolls being performed throughout the test, $C_{y\beta}$ is frequently observable and the Kalman filter is able to maintain an accurate converged solution resulting in a good estimation of AOS, within roughly 0.6 degrees of error. AOA estimation is poor due to the lack of visibility of $C_{z\alpha}$.

This method's highest performance for AOS estimation is in steady state sideslip tests. AOS error is roughly within 0.6 degrees, and could potentially be used as an alternative to the traditional methods

for this test case. On the other hand, AOA estimates for this test are poor, due to the fact that there is little visibility of $C_{z\alpha}$.

4.3 Correlation

It is important to notice the amount of correlation seen between this method's estimated air flow angles and the traditional methods' air flow angles. It should be noted that there is significant possibility of error in the traditional measurements of the air flow angles, which are largely assumed to be the correct answer for this study. Some of the errors attributed to this method may actually be errors in the traditional methods it is being compared to, thus making this method more accurate for some scenarios. Even when the two answers differ significantly, resulting in a high error for this method, the correlation of the curves is still seen. This is important because it shows the validity of this method, and the potential for it to be improved in the future. The estimation of the stability derivatives by this method closely match previously studied measurements of the stability derivatives for this aircraft, bringing higher confidence in this new method's results.¹⁰ In addition, the stability derivatives significantly change when the aircraft configuration is changed, i.e when the gear is down we see a change in $C_{y\beta}$ as expected.

4.4 Wind Estimation

A very important source of error for this method of measuring air flow angles, is in the estimation of the wind itself. This method currently uses a moving window of air data and a computationally intense method to converge an instantaneous estimation of wind velocity. Wind is inherently difficult to measure from within an aircraft, and the error associated with this method depends greatly on steady winds. If wind velocities are changing significantly over short periods of time, then the method for wind estimation becomes less accurate. The error associated with this wind estimation more regularly affects AOS estimations. AOA estimations are not affected as often, because AOA estimations depend primarily on vertical wind speed only and this is generally considered to be negligible.

4.5 Future research

This method has shown a great deal of promise, but still has necessary work before it will be a viable solution to replace the traditional methods for a flight test program. First, improvements in wind estimation would make this method more robust. Real-time wind estimation is difficult to employ, but

could replace the moving window of air data method currently used. In addition, ensuring testing is performed in steady wind or calm days would be beneficial in obtaining accurate results.

The method for estimation of air flow angles currently is used in post-processing of flight test data. However, the algorithms developed were based on a real-time scenario, and would take minimal work to port to a real-time user platform. Real-time implementation of this method is a valid goal, and would likely be simple to accomplish. This would be beneficial for flight test engineers to compare this to the traditional methods in flight.

Currently, only discrete Kalman Filters are used in this method. Use of a Complementary Kalman Filter holds the potential to greatly increase the accuracy if tuned properly. The complementary filter would be able to use multiple methods for estimating the air flow angles simultaneously and weigh each of these methods in the filter. This means that if it is known that one method works well for a certain flight condition, this method would get a higher weight for that flight condition; when the flight condition changes, the weights of the methods would change in the filter. This multiple input method would allow the filter to converge to a more accurate solution than any single input.

Recently, Dr. Morelli has reported on the concept of using inertial measurements to perform real-time parameter identification without air flow angles. His work uses data in the frequency domain, enabling aerodynamic parameter estimation without directly measured air flow angles. Bias and scale errors are removed by filtering in the frequency domain, yielding excellent results of the aerodynamic stability derivatives. It should be possible to expand on Dr. Morelli's work, using his method to estimate the stability derivatives, and combine it with work from this thesis to achieve a greater accuracy in the reconstruction of air flow angles.¹¹

5. REFERENCES

- [1] Lawford, J. A., and K. R. Nippess. "Calibration of Air-Data Systems and Flow Direction Sensors." *AGARD Flight Test Techniques Series; AG-300 1* (1984).
- [2] Colgren, Richard D. "The Feasibility of Using an INS for Control System Feedbacks." *American Institute of Aeronautics and Astronautics* (1998). Lockheed Martin Skunk Works.
- [3] Colgren, Richard D., and Keith E. Martin. "Flight Test Validation Of Sideslip Estimation Using Inertial Accelerations." *AIAA Guidance, Navigation, and Control Conference and Exhibit AIAA-2000-4448* (2000). American Institute of Aeronautics and Astronautics, Inc.
- [4] Colgren, Richard D., Michael T. Frye, and Wayne M. Olson. "A Proposed System Architecture For Estimation Of Angle-Of-Attack And Sideslip Angle." *AIAA-99-4078* (1999). American Institute of Aeronautics and Astronautics, Inc.
- [5] Klein, Vladislav, and Eugene A. Morelli. *Aircraft System Identification: Theory and Practice*. Reston, VA: American Institute of Aeronautics and Astronautics, 2006. Print.
- [6] Welch, Greg, and Gary Bishop. "An Introduction to the Kalman Filter." *SIGGRAPH Course 8* (2001). University of North Carolina at Chapel Hill Department of Computer Science.
- [7] Zarchan, Paul, and Howard Musoff. "Appendix B." *Fundamentals of Kalman Filtering a Practical Approach*. Reston, Va: American Institute of Aeronautics and Astronautics, 2000.
- [8] Rajnicek, Rachel E. "Application Of Kalman Filtering To Real-Time Flight Regime Recognition Algorithms In A Helicopter Health And Usage Monitoring System." *Embry-Riddle Aeronautical University; Daytona Beach, Florida* (2008).

- [9] Anderson, Richard P. *Level 6 Flight Test Report For The Diamond DA42*. Tech. Daytona Beach, FL: Embry-Riddle Aeronautical University, 2007.
- [10] Londono, Monica M. "Determination Of Stability And Control Derivatives For A Modern Light Composite Twin Engine Airplane." *Embry-Riddle Aeronautical University; Daytona Beach, Florida* (2009).
- [11] Morelli, Eugene A. "Real-Time Aerodynamic Parameter Estimation without Air Flow Angle Measurements." AIAA 2010-7951 (2010). American Institute of Aeronautics and Astronautics, Inc.

APPENDIX A: TEST NAMING SCHEME

Sect.	Name	Description/Configuration	Filename
1a1	Ground Acceleration	Takeoff	1a1_1
1b1	Normal Climb	2 nd Segment Climb	1b1_1
1b2	One Engine Inoperative Climb	2 nd Segment Climb	1b2_1
1c2	Stall Warning Actuation	2 nd Segment Climb	1c2_1
		Approach	1c2_4
		Landing	1c2_7
1d1	Stopping Time, Heavy Braking	Landing	1d1_1
1e1	Engine Acceleration	Landing	1e1_1
1e2	Engine Deceleration	Takeoff	1e2_1
2a1	Stick Position vs. Force and Surface Position Calibration (Pitch)	Ground, Pitch Control	2a1_1
2a2	Stick Position vs. Force and Surface Position Calibration (Roll)	Ground, Roll Control	2a2_1
2a3	Rudder Position vs. Force and Surface Position Calibration (Yaw)	Ground, Yaw Control	2a3_1
2a5	Rudder Pedal Steering Calibration	Ground	2a5_1
2a6	Pitch Trim Calibration	Ground	2a6_1
2a7	Alignment of Power Lever Angle	Ground, Full Forward	2a7_1
2a8	Brake Pedal Calibration	Ground	2a8_1
2c1b	Power Change Force	Cruise, Decelerate	2c1ba1
		Cruise, Accelerate	2c1bb1
		Approach, Decelerate	2c1bc1
		Approach, Accelerate	2c1bc2
2c2	Flap Change Force	Retraction, Gear Up	2c2-a1u
		Retraction, Gear Down	2c2-a1d
		Extension, Gear Up	2c2-b2
		Extension, Gear Down	2c2-b3
2c4	Gear Change Force	Retraction, No Flaps	2c4a1
		Retraction, Flaps 50%	2c4a4
		Retraction, Flaps 100%	2c4a7
		Extension, No Flaps	2c4b1
		Extension, Flaps 50%	2c4b4
		Extension, Flaps 100%	2c4b7
2c5	Gear and Flap Operational Time	Retraction, No Flaps	2c4a1
		Retraction, Flaps 50%	2c4a4
		Retraction, Flaps 100%	2c4a7
		Extension, No Flaps	2c4b1
		Extension, Flaps 50%	2c4b4
		Extension, Flaps 100%	2c4b7
		Retraction, Gear Down	2c2-12
		Extension, Gear Up	2c2-22u
		Extension, Gear Up	2c2-22d

Sect.	Name	Description/Configuration	Filename
2c6	Longitudinal Trim	No Flaps, Gear Up	2c6a1maxa
			2c6a1maxb
			2c6a1maxc
			2c6a1140a
			2c6a1140b
			2c6a1140c
			2c6a1130a
			2c6a1130b
			2c6a1130c
			2c6a1120a
			2c6a1120b
			2c6a1120c
			2c6a1110a
			2c6a1110b
			2c6a1110c
			2c6a1100a
			2c6a1100b
			2c6a1100c
			2c6a190a
			2c6a190b
			2c6a190c
			2c6a185a
			2c6a185b
			2c6a185c
			2c6a180a
			2c6a180b
			2c6a180c
			2c6a175a

Sect.	Name	Description/Configuration	Filename
2c6	Longitudinal Trim	No Flaps, Gear Up	2c6a175b
			2c6a175c
			2c6a170a
			2c6a170b
			2c6a170c
		Flaps 50%, Gear Up	2c6a2maxa
			2c6a2maxb
			2c6a2maxc
			2c6a2110a
			2c6a2110b
			2c6a2110c
			2c6a2100a
			2c6a2100b
			2c6a2100c
			2c6a290a
			2c6a290b
			2c6a290c
			2c6a285a
			2c6a285b
			2c6a285c
			2c6a280a
			2c6a280b
			2c6a280c
			2c6a275a
			2c6a275b
			2c6a275c
			2c6a270a
			2c6a270b
			2c6a270c
			2c6a265a
			2c6a265b
			2c6a265c
			2c6a2mina
			2c6a2minb
			2c6a2minc
		Flaps 100%, Gear Up	2c6a3maxa
			2c6a3maxb
			2c6a3maxc
			2c6a390a
			2c6a390b
			2c6a390c
			2c6a385a
			2c6a385b
			2c6a385c
			2c6a380a
			2c6a380b
			2c6a380c
			2c6a375a
			2c6a375b
			2c6a375c
			2c6a370a

Sect.	Name	Description/Configuration	Filename
2c6	Longitudinal Trim	Flaps 100%, Gear Up	2c6a370b
			2c6a370c
			2c6a365a
			2c6a365b
			2c6a365c
			2c6a360a
			2c6a360b
			2c6a360c
		No Flaps, Gear Down	2c6a4maxa
			2c6a4maxb
			2c6a4maxc
			2c6a4110a
			2c6a4110b
			2c6a4110c
			2c6a4100a
			2c6a4100b
			2c6a4100c
			2c6a490a
			2c6a490b
			2c6a490c
			2c6a485a
			2c6a485b
			2c6a485c
			2c6a480a
			2c6a480b
			2c6a480c
			2c6a475a
			2c6a475b
			2c6a475c
			2c6a470a
			2c6a470b
			2c6a470c
			2c6a4mina
			2c6a4minb
			2c6a4minc
		Flaps 50%, Gear Down	2c6a5maxa
			2c6a5maxb
			2c6a5maxc
			2c6a5100a
			2c6a5100b
			2c6a5100c
			2c6a590a
			2c6a590b
			2c6a590c
			2c6a585a
			2c6a585b
			2c6a585c

Sect.	Name	Description/Configuration	Filename
2c6	Longitudinal Trim	Flaps 50%, Gear Down	2c6a580a
			2c6a580b
			2c6a580c
			2c6a575a
			2c6a575b
			2c6a575c
			2c6a570a
			2c6a570b
			2c6a570c
			2c6a565a
			2c6a565b
			2c6a565c
			2c6a560a
			2c6a560b
			2c6a560c
		Flaps 100%, Gear Down	2c6a6maxa
			2c6a6maxb
			2c6a6maxc
			2c6a685a
			2c6a685b
			2c6a685c
			2c6a680a
			2c6a680b
			2c6a680c
			2c6a675a
			2c6a675b
			2c6a675c
			2c6a670a
			2c6a670b
			2c6a670c
			2c6a665a
			2c6a665b
			2c6a665c
			2c6a660a
			2c6a660b
			2c6a660c
			2c6a655a
			2c6a655b
			2c6a655c
2c7	Longitudinal Maneuvering	Cruise	2c7a1
		Approach	2c7b4
		Landing	2c7c4
2c8	Longitudinal Static Stability	Approach	2c8a1
2c9	Phugoid Dynamics	No Flaps, Gear Up	2c9a1u
		No Flaps, Gear Down	2c9a1d
2c10	Short Period	Cruise	2c10a11

Sect.	Name	Description/Configuration	Filename
2d1	Minimum Control Speed	Landing, Left Engine Out	2d1a11
			2d1a12
			2d1a13
		Landing, Right Engine Out	2d1a21
			2d1a22
			2d1a23
		Takeoff, Left Engine Out	2d1b11
2d2	Roll Response	Takeoff, Right Engine Out	2d1b21
		Cruise, Left Bank	2d2a21
		Cruise, Right Bank	2d2a22
		Approach, Left Bank	2d2b11
		Approach, Right Bank	2d2b12
		Landing, Left Bank	2d2c21
		Landing, Right Bank	2d2c22
2d3	Response to Roll Control Step Input	Approach, Right Step Input	2d3b21
		Approach, Left Step Input	2d3b22
2d4b	Spiral Stability	Cruise, Right Bank	2d4a21
		Cruise, Left Bank	2d4a22
		Approach, Right Bank	2d4b21
		Approach, Left Bank	2d4b22
		Landing, Right Bank	2d4c21
		Landing, Left Bank	2d4c22
2d6	Rudder Response	Approach, Right Rudder	2d6a11
		Approach, Left Rudder	2d6a12
		Landing, Right Rudder	2d6a11d
		Landing, Left Rudder	2d6a12d
2d7	Dutch Roll	Cruise	2d7a1
		Approach	2d7b2
		Landing	2d7c2
2d8	Steady State Sideslip	No Flaps, Gear Up, Left Sideslip	2d8a1
		No Flaps, Gear Up, Left Sideslip w. trim	2d8a1_trim
		No Flaps, Gear Up, Right Sideslip	2d8a2
		No Flaps, Gear Up, Right Sideslip w. trim	2d8a2_trim
		No Flaps, Gear Down, Left Sideslip	2d8b1
		No Flaps, Gear Down, Right Sideslip	2d8b2
		50% Flaps, Gear Up, Left Sideslip	2d8d1
		50% Flaps, Gear Up, Right Sideslip	2d8d2
		50% Flaps, Gear Down, Left Sideslip	2d8e1
		50% Flaps, Gear Down, Left Sideslip w. trim	2d8e1_trim
		50% Flaps, Gear Down, Right Sideslip	2d8e2
		50% Flaps, Gear Down, Right Sideslip w. trim	2d8e2_trim
		100% Flaps, Gear Up, Left Sideslip	2d8f1
		100% Flaps, Gear Up, Right Sideslip	2d8f2
		100% Flaps, Gear Down, Left Sideslip	2d8g1
		100% Flaps, Gear Down, Left Sideslip w. trim	2d8g1_trim
		100% Flaps, Gear Down, Right Sideslip	2d8g2
		100% Flaps, Gear Down, Right Sideslip w. trim	2d8g2_trim



THESIS BINDING AND SHIPPING FORM

TO: Acquisitions Librarian, Hunt Library

DATE: _____

FROM: Associate Vice President for Academics

STUDENT NAME: _____

DEGREE: _____

DATE CONFERRED: _____

THESIS TITLE: _____

_____ NUMBER OF COPIES TO BE BOUND @ \$20.00 EACH TOTAL \$ _____

CREDIT LIBRARY BINDING ACCOUNT: 22510-7299

(The Library requires **two print copies** for the Library's collection. Please provide a copy of the thesis on a CD-ROM or USB drive, also. The Library recommends the thesis be printed on 20# weight white paper stock.)

APPROVAL:

SIGNATURE: _____

Associate Vice President for Academics (signature)

PRINT NAME: _____ DATE: _____

IF COPIES ARE TO BE MAILED, PLEASE COMPLETE ADDRESS DETAILS BELOW:

PLEASE NOTE: Library will mail copies to one address only.

NAME: _____

ADDRESS: _____

TELEPHONE: _____

_____ NUMBER OF COPIES TO BE MAILED **INSIDE** UNITED STATES @ \$5.00 EACH TOTAL \$ _____

_____ NUMBER OF COPIES TO BE MAILED **OUTSIDE** UNITED STATES @ \$25.00 EACH TOTAL \$ _____

(Must include completed Customs forms.)

CREDIT LIBRARY SHIPPING ACCOUNT: 22510-7240

Other Instructions: _____